Rapid adaptation of endocytosis, exocytosis and eisosomes after an acute increase in membrane tension in yeast cells

Joël Lemière[a, b, d *], Yuan Ren[a, b, *], Julien Berro[a, b, c, §]

[a] Department of Molecular Biophysics and Biochemistry, Nanobiology Institute, Yale University, New Haven, CT, USA
[b] Nanobiology Institute, Yale University, West Haven, CT 06516, USA
[c] Department of Cell Biology, Yale University School of Medicine, New Haven, CT 06520, USA
[d] Current address: UCSF, Department of Cell and Tissue Biology, San Francisco, CA, USA
[*] Authors contributed equally
[§] Contact: julien.berro@yale.edu

Abstract

During clathrin-mediated endocytosis in eukaryotes, actin assembly is required to overcome large membrane tension and turgor pressure. However, the molecular mechanisms by which the actin machinery adapts to varying membrane tension remain unknown. In addition, how cells reduce their membrane tension when they are challenged by hypotonic shocks remains unclear. We used quantitative microscopy to demonstrate that cells rapidly reduce their membrane tension using three parallel mechanisms. In addition to using their cell wall for mechanical protection, yeast cells disassemble eisosomes to buffer moderate changes in membrane tension on a minute time scale. Meanwhile, a temporary reduction of the rate of endocytosis for 2 to 6 minutes, and an increase in the rate of exocytosis for at least 5 minutes allow cells to add large pools of membrane to the plasma membrane. We built on these results to submit the cells to abrupt increases in membrane tension and determine that the endocytic actin machinery of fission yeast cells rapidly adapts to perform clathrin-mediated endocytosis. Our study sheds light on the tight connection between membrane tension regulation, endocytosis and exocytosis.

Introduction

During clathrin-mediated-endocytosis (CME), the cell plasma membrane undergoes a dramatic change in topology to form an invagination that is subsequently pinched off into a vesicle. During this process, the endocytic machinery has to overcome the forces produced by membrane tension and the osmotic pressure that oppose membrane deformation and engulfment. In yeast cells, these resisting forces are particularly large because their internal turgor pressure is high, ranging from ~0.6 MPa for *Saccharomyces cerevisiae* to more than 1 MPa for *Schizosaccharomyces pombe* (Davì et al., 2018; Minc et al., 2009; Schaber et al., 2010). Consequently the formation of a vesicle requires several thousands of pN (Dmitrieff and Nédélec, 2015; Ma and Berro, 2021).

Previous studies have shown that actin dynamics is required for productive endocytosis in yeast (Aghamohammadzadeh et al., 2014; Basu et al., 2013; Carlsson and Bayly, 2014; Palmer et al., 2015) and in mammalians cells when membrane tension is high (Aghamohammadzadeh and Ayscough, 2009; Boulant et al., 2011; Hassinger et al., 2017), or when membrane scission proteins are absent (Ferguson et al., 2009). Actin assembly at the endocytic site is believed to provide the forces that overcome turgor pressure and membrane tension to deform the plasma membrane, but the precise mechanisms of force production remain unknown (reviewed in Berro and Lacy, 2018; Goode et al., 2015; Lacy et al., 2018). We also lack a quantitative understanding of the regulation of actin dynamics in response to membrane tension and turgor pressure changes. We expect that a better quantitative characterization of this response will allow us to infer the molecular mechanisms of force production and force sensing during clathrin-mediated endocytosis.

The mechanisms by which membrane tension is regulated are not fully understood. The yeast cell wall is believed to buffer abrupt changes in turgor pressure thanks to its high stiffness of ~50 MPa (Atilgan et al., 2015). In addition, similarly to mammalian cells' caveolae which change shape or disassemble in response to increased membrane tension, yeast eisosomes can also disassemble when cells without a cell wall, called protoplasts, are placed in low osmolarity media (Kabeche et al., 2015; Parton et al., 2019; Sinha et al., 2011). However, it remains unknown how eisosomes may regulate plasma membrane tension in intact cells, and whether eisosome disassembly directly influences cellular processes such as CME. In addition, it remains unclear to which extent endocytosis and exocytosis may contribute to the regulation of membrane tension when the cells are challenged with an abrupt increase in membrane tension.

Fission yeast is an ideal model system to quantitatively study the regulation mechanisms of membrane tension and its influence on the endocytic machinery. First, because yeast turgor pressure is high, actin is required for CME. Second, contrary to mammalian cells, yeast cells are devoid of any adhesion machinery or actin cortex, which usually complicates membrane tension manipulation and result interpretation. Last, quantitative microscopy methods developed in fission yeast are able to uncover fine regulations of the endocytic machinery and precisely measure the local and global numbers of endocytic events at a given time (Arasada and Pollard, 2011; Berro et al., 2010; Berro and Lacy, 2018; Berro and Pollard, 2014a, 2014b; Chen and Pollard, 2013; Lacy et al., 2019; Sirotkin et al., 2010).

To probe the contributions of each possible mechanism of membrane tension regulation and their influence on CME, we submitted yeast cells with or without a cell wall to different hypotonic shocks. Using quantitative fluorescence microscopy, we showed that, on the one hand, yeast cells rapidly reduce their membrane tension by a) disassembling eisosomes, b) reducing their rate of endocytosis and c) increasing their rate of exocytosis, and, on the other hand, actin assembly adapts to increased membrane tension to allow endocytosis to proceed.

Results

Eisosomes participate in the regulation of protoplasts' membrane tension

Previous studies proposed that eisosomes, furrows at the inner surface of the plasma membrane, have a mechanoprotective role under increased membrane tension in fungi by acting as a reservoir of membrane, similar to the protective role of caveolae in endothelial cells (Cheng et al., 2015; Kabeche et al., 2015; Lo et al., 2016; Sens and Turner, 2006; Sinha et al., 2011). Since the yeast cell wall plays a major role in the maintenance of cell integrity under extreme osmotic conditions, thanks to its high stiffness of ~50 MPa (Atilgan et al., 2015), it prevents large variations in membrane tension under hypotonic shocks. Hence, to exclude the effect of the cell wall and amplify membrane tension changes, we performed our experiments using cells devoid of a cell wall, hereafter referred to as "protoplasts", instead of intact cells, hereafter referred to as "walled cells"

First, we characterized how the removal of the cell wall affects eisosomes' reorganization. We used a protocol that allowed us to manipulate protoplasts for up to ~1 hour after their formation, since they remain void of cell wall for about 3 hours (Flor-Parra et al., 2014). Because protoplasts are more fragile than walled cells, they were prepared in Edinburgh Minimum Media (EMM5S) containing 0.25 to 1.2 M sorbitol to balance turgor pressure and prevent cells from bursting, while keeping nutrient concentration constant (Basu et al., 2013; Kabeche et al., 2015; Stachowiak et al., 2014), and were imaged ~15 minutes later, once they reached steady state. In the rest of the paper, we will refer to this experimental condition as "steady state in X M" or "chronic exposure to X M sorbitol", where X is the sorbitol concentration.

Our data show that eisosomes in protoplasts at steady state in 1.2 M sorbitol are qualitatively similar to those in walled cells (Figure 1A) and the cellular concentration of Pi1lp is the same in both conditions (Figure 1E). However, the surface area of the protoplasts' plasma membrane covered by eisosomes decreased with decreasing media osmolarity at steady state (Figures 1B and 1C) and correlated with increasing cell volume (Figure 1D). This result confirms previous results (Kabeche et al., 2015) showing that eisosomes are disassembled in media with low osmolarity and the disassembly of eisosomes may reduce membrane tension.

We then performed hypotonic shocks to abruptly increase the membrane tension of protoplasts and we imaged them before their long-term adaptation to changes in media osmolarity. Prior to the shocks, we let cells reach steady state by exposing them to media with a given sorbitol concentrations for more than 15 minutes. We chose 0.4 M sorbitol as the steady state concentration for this experiment as it corresponds to the estimated turgor pressure of walled cells (~1 MPa) and at this concentration the dynamics of the actin endocytic machinery was virtually identical to the one in walled cells (Figure 7 – Supplement 1B). We performed acute hypotonic shocks by using a microfluidic system to rapidly exchange the steady state media with media containing a lower sorbitol concentration, hereafter noted ΔC=-Y M where Y is the difference in media osmolarity (note that the change in pressure ΔP in Pascal is related to the change in osmolite concentration ΔC in Molar as $\Delta P = \Delta C \cdot RT \sim 2.45 \cdot 10^6 \cdot \Delta C$, where R is the gas constant and T the absolute temperature, when the solute concentration is sufficiently low).

To quantitatively characterize eisosome disassembly in protoplasts after a hypotonic treatment, we measured the temporal evolution of the decrease in surface area covered by eisosomes after an acute hypotonic shock of ΔC=-0.2 M starting with protoplasts at steady state in 0.4 M sorbitol (Figure 1H and 1I). Eisosomes disassembled rapidly after hypotonic shock, dropping to ~50% of the surface area covered by eisosomes before the shock within 5 min, indicating a fast response to counteract the hypotonic shock and an eventual change in membrane tension.

To test whether membrane tension is buffered by eisosomes, we measured membrane tension using a micropipette aspiration assay (Figure 1F). At steady state in 0.8 M sorbitol, the membrane tension was 0.45±0.14 $mN \cdot m^{-1}$ for wild-type protoplasts and 0.39±0.13 $mN \cdot m^{-1}$ for *pil1Δ* protoplasts (Figure 1G). We then repeated these measurements within 5 minutes after inducing a hypotonic shock of ΔC=-0.2 M. We observed a 1.6-fold increase in membrane tension for wild-type protoplasts (0.73±0.21 $mN \cdot m^{-1}$) and a 4.5-fold increase for protoplasts lacking eisosomes (1.74±0.61 $mN \cdot m^{-1}$). This result demonstrates that eisosomes participate in the adjustment of plasma membrane tension.

In protoplasts, eisosomes buffer moderate hypotonic shocks

Since WT protoplasts were able to withstand osmotic shocks by disassembling their eisosomes, we hypothesized that protoplasts lacking eisosomes – either because they lack the core eisosome protein Pil1p or because eisosomes are mechanically removed – are more sensitive to hypotonic shocks.

WT and *pil1Δ* protoplasts initially at steady state in 0.4 M sorbitol survived small hypotonic shocks (ΔC=0.05 M) equally well (Figure 2A). However, *pil1Δ* protoplasts were more sensitive to moderate hypotonic shocks (ΔC=0.1 M) since most of them were unable to survive two minutes after the moderate shock while virtually all the WT protoplasts were able to survive (Figure 2B, Figure 2 – Supplement 1).

Moreover, eisosomes were unable to protect protoplasts from larger hypotonic shocks (ΔC=0.2 M), where most eisosomes are disassembled (Figures 1H and 1I) since most wild-type protoplasts were unable to survive longer than 4 minutes after these high hypotonic shocks, similarly to *pil1Δ* protoplasts (Figure 2C). To further confirm increased death rate was due to the lack of eisosomes, we performed a moderate shock (ΔC=0.1 M) on protoplasts originally at steady-state in 0.25 M sorbitol where eisosomes are mostly disassembled already. Under these conditions, WT protoplasts survival was comparable to the survival of *pil1Δ* (Figure 2D). This result further demonstrates that the presence of assembled eisosomes at the plasma membrane is indeed responsible for the adaptation of cells to acute hypotonic shocks, and the presence of Pil1p in the cytoplasm is not sufficient for this response.

Altogether, these experiments demonstrate that a) eisosomes protect protoplasts from changes in their membrane tension, but only to a small extent, b) without eisosomes, protoplasts can withstand only minor increase in their membrane tension.

Eisosomes protect the integrity of walled cells during consecutive osmotic shocks

We observed that a significant number of both wild-type and *pil1Δ* protoplasts died after osmotic shocks, and the percentage of *pil1Δ* protoplasts that remained alive was significantly smaller than for wild-type protoplasts even under moderate shocks ΔC of -0.05 M, -0.1 M and -0.2 M (Figures 2A-C). In contrast, we found that both wild-type and *pil1Δ* walled cells can survive a single osmotic shock of ΔC=-1.2 M, which initially led us to think that eisosomes only have a minor protective role in walled cells (Figure 2F). However, we noticed that subsequent osmotic shocks led to a higher mortality of *pil1Δ* compare to wild-type walled cells. While almost all the wild-type walled cells remained alive after several shocks, around 10% of *pil1Δ* walled cells died after each subsequent shock (Figures 2E,2F and 2G; supplementary video 1 and 2). These results demonstrate that, even in walled cells, eisosomes exert a protective role, likely by buffering sudden changes in membrane tension.

Membrane tension and eisosomes modulate the rate of endocytosis in cells

Within a few minutes of a hypotonic shock, the volume of WT protoplasts increased up to 50% and the volume of *pil1Δ* protoplasts increased up to 20% (Figures 3A and 3B, insets). However, the corresponding increase in surface area cannot be explained by eisosome disassembly alone – total eisosome disassembly could release about 5% of the total surface area of the plasma membrane, assuming eisosomes are hemi-cylinders with diameter ~50 nm and cells contain 1.6 μm of eisosomes per μm^2 of plasma membrane on average (Kabeche et al., 2015). Therefore, another mechanism for protoplasts to gain plasma membrane occurs in the first few minutes after hypotonic shocks. We hypothesized that a decrease in the number of endocytic events happening in the cell after a hypotonic shock would gradually increase the surface area of the plasma membrane and reduce membrane tension.

We measured the endocytic density, i.e. the number of endocytic events in a cell normalized by the cell length, in wild-type and *pil1Δ* cells after a hypotonic shock using a ratiometric method (Berro and Pollard, 2014a). In brief, this method consists of imaging cells expressing a fluorescently tagged endocytic protein, here the actin filament crosslinking protein fimbrin (Fim1p) tagged with a monomeric enhanced green fluorescent protein (mEGFP), hereafter called Fim1p-mEGFP. First, we measure the temporal average intensity of the fluorescent protein at endocytic sites. Second, we measure the whole intensity of each cells from which the corresponding cytoplasmic intensity is subtracted – this number represents the sum of the intensities for all the fluorescently tagged proteins present at endocytic sites. The number of endocytic sites in each cell is then calculated as the ratio between those two numbers. The endocytic density is calculated by dividing this ratio with the cell length.

For all shocks tested in wild-type (ΔC=-0.05 M, -0.1 M, -0.2 M) and *pil1Δ* protoplasts (ΔC=-0.025 M, -0.05 M, -0.1 M) initially at steady state in 0.4 M sorbitol, the endocytic density in protoplasts significantly decreased immediately after the hypotonic shock (Figure 3A). The difference increased for increasing hypotonic shocks, up to 36% for wild-type protoplasts after a ΔC=-0.2 M shock, and 79% for *pil1Δ* protoplasts after a ΔC=-0.1 M shock (Figure 3B). These abrupt changes in the endocytic density were followed by a 2- to 6-minute recovery back to the steady-state endocytic density, and recovery time depended on the magnitude of the hypotonic shock. Note that the change in cell volume (Figures 3A and 3B, insets) could not exclusively account for the observed decrease in the endocytic density in wild-type cells as the relative increase in cell volumes were larger than the relative decrease in endocytic density 2 minutes after the shocks and remained large 4 minutes after while the endocytic densities recovered their pre-shock values.

Building on these results in protoplasts, we wondered whether the endocytic density in walled cells also adapts to hypotonic shocks. Indeed, immediately after the largest shock tested (ΔC=-1.2 M), we observed a similar decrease in the endocytic density for both wild-type and *pil1Δ* walled cells, 36% and 46% respectively (Figure 3D). Recovery to steady-state endocytic densities occurred in less than 2 minutes in both wild-type and *pil1Δ* walled cells, faster than in protoplasts (Figures 3A, 3B and

3D). Our data show that the cell wall limits but does not completely cancel the effect of hypotonic shocks on endocytic rates. They also suggest that the regulation of the endocytic density supplements the regulation performed by the eisosomes to reduce membrane tension.

Wild-type and *pil1Δ* walled cells had a very similar adaptation after hypotonic shocks. However, we noticed a difference in the endocytic density at steady state in different sorbitol concentrations. For all concentrations tested (0 to 2 M), wild-type cells maintained roughly the same endocytic density. In contrast, the steady state endocytic density in *pil1Δ* cells increased with increasing media osmolarity, up to 56% in 2 M sorbitol (Figure 3C). Our results suggest that eisosomes participate in maintaining a constant density of endocytosis independently of the media osmolarity, not only after an abrupt change in membrane tension, but also when they are at steady state in different osmolarity.

The exocytosis rate increases after a hypotonic shock in protoplasts but not in walled cells

Reciprocal to the decrease in the number of endocytic events observed after a hypotonic shock, we wondered whether the rate of exocytosis increases in the meantime to provide more surface area to the plasma membrane, as has been observed in mammalian cells (Gauthier et al., 2009).

To measure the rate of exocytosis in different conditions, we used the cell impermeable styryl dye FM4-64, whose fluorescence dramatically increases when it binds to membranes (Cochilla et al., 1999; Gachet and Hyams, 2005; Richards et al., 2000). After FM4-64 is introduced to the media, the plasma membrane is rapidly stained (Figure 4A). Fusion of unstained intracellular vesicles to the plasma membrane results in an increase of total cell fluorescence, because after each fusion event new unstained membrane from the interior of the cell is exposed to the dye. At this stage, if one wanted to measure endocytosis rates, one would typically remove the FM4-64 dye from the media to destain the plasma membrane, and quantify the internal fluorescence which is proportional to the amount of membrane internalized by endocytosis. Here, we kept the FM4-64 dye in the media, and monitored the fluorescence of the plasma membrane and the interior of the cell. In this case, endocytic events do not increase the total cell fluorescence because they transfer patches of the plasma membrane that are already stained into the interior of the cell (Figure 4A, red arrow). Therefore, the increase in fluorescence we measured is due to the addition of new unstained lipids to the plasma membrane by exocytosis (Figure 4A, gray arrow). Note that the increase in total cell fluorescence could also be due to putative transfer of lipids by non-exocytic mechanisms (Reinisch and Prinz, 2021) but for simplicity and by lack of further evidence, onwards we will interpret the increase in fluorescence to an increase in the exocytosis rate.

Staining of wild-type fission yeast with 20 µM FM4-64 in EMM5S (Figure 4B) showed that after a brief phase of rapid staining of the cell surface, the total cell fluorescence intensity grows roughly linearly for at least 20 minutes, and the slope of the normalized intensity corresponds to the exocytosis rate as a percentage of the plasma membrane surface area per unit of time (see materials and methods) (Gauthier et al., 2009; Smith and Betz, 1996; Vida and Emr, 1995). Using this method, we measured that wild-type walled cells at steady state in EMM5S exocytose 4.6% of their plasma membrane surface area per minute (Figure 4B). FM4-64 staining did not seem to affect the endocytic and exocytic membrane trafficking of yeast cells, since stained vesicles are successfully released after washing cells with fresh media (Figure 4B).

We measured the exocytosis rates in the conditions that had the largest effects on the rates of endocytosis while keeping most cells alive, i.e. we used protoplasts at steady state in 0.4 M and performed a $\Delta C=-0.2$ M shock for wild-type and $\Delta C=-0.05$ M shock for *pil1Δ*. At steady state in 0.4M sorbitol (Figures 4F and 4H), wild-type protoplasts had an exocytosis rate similar to walled cells in EMM5S in 0 M ($k_{0-5}=4.4\pm0.2\%$ min^{-1}). After a $\Delta C=-0.2$ M shock, the exocytosis rate increased by 41% ($k_{0-5}=6.2\pm0.4\%$ min^{-1}). At steady state in 0.4 M sorbitol (Figures 4G and 4H), the exocytosis rate of *pil1Δ* protoplasts was higher than for walled cells in 0 M sorbitol ($k_{0-5}=6.2\pm0.4\%$ min^{-1}). After a $\Delta C=-0.05$ M shock, the exocytosis rate increased modestly ($k_{0-5}=6.8\pm0.5\%$ min^{-1}). Therefore, in both wild-type and *pil1Δ* protoplasts, an acute hypotonic shock leads to an increased exocytosis rate, which increases surface area and likely reduces membrane tension. The change in exocytosis rate in *pil1Δ* protoplasts being more modest than in wild-type cells highlights the role of eisosomes in buffering the change in the exocytosis rate in response to change in osmolarity and membrane tension.

We wondered whether these changes in exocytosis rate also happen in walled cells. First, we measured exocytosis rate at steady state in solutions with different molarities and found that the rates were smaller than in protoplasts (Figures 4C-E). The exocytosis rate of wild-type walled cells at steady state in 1.2M sorbitol ($k_{0-5}=3.1\pm0.1$ % min^{-1}, Figures 4C and 4E) was 35% smaller than in 0 M sorbitol ($k_{0-5}=4.8\pm0.1$ % min^{-1}, Figure 4B). In addition, in *pil1Δ* walled cells, the exocytosis rate of walled cells lacking eisosomes in 1.2M sorbitol was only slightly smaller than wild-type cells in the same conditions ($k_{0-5}=2.6\pm0.1$ % min^{-1}, Figures 4D and 4E). After hypotonic shocks, the change of exocytosis rate in walled cells was very limited (Figures 4C-E). In fact, our strongest hypotonic shock of $\Delta C=-1.2$ M did not significantly increase the exocytosis rate of wild-type or *pil1Δ* cells walled cells (Figure 4E). These data corroborate our previous finding that the cell wall limits but does not completely cancel the effect of hypotonic shocks in intact cells. In addition, they also demonstrate that eisosomes are involved in the regulation of the exocytosis rate.

Inhibition of exocytosis decreased the survival rate of protoplasts under acute hypotonic shock and inhibition of endocytosis increased their survival rate

To further test our hypothesis that reducing the endocytosis rate and increasing the exocytosis rate help regulate membrane tension after a hypotonic shock, we blocked endocytosis or exocytosis with drugs and measured the survival rates of cells. We hypothesized that inhibition of endocytosis or exocytosis would have opposite effects on the survival of protoplasts under acute hypotonic shock. Specifically, inhibition of endocytosis would help retain membrane on the surface of protoplasts, thereby reducing the probability of membrane rupture. Conversely, inhibition of exocytosis would reduce the transfer of membrane from intracellular vesicles to the surface of protoplasts, exacerbating the lack of plasma membrane in the face of imminent protoplast expansion. To observe the largest effects, we used *pil1Δ* protoplasts under $\Delta C=-0.2$ M shock and exposed the cells to either Latrunculin A (LatA) or Brefeldin A (BFA) for 30 minutes before the shocks.

Blocking exocytosis with BFA increased the death rate of protoplasts after hypotonic shocks, confirming our hypothesis (Figure 5). Blocking actin assembly, and therefore endocytosis, with LatA made the protoplasts more resistant starting 4 minutes after the hypotonic shock, also confirming our hypothesis. Note that LatA treatment made the protoplasts less resistant to shock in the initial 2 minutes after the hypotonic shock, which seems in contradiction with our hypothesis. However, it is possible that prolonged treatment with LatA had other unidentified effects on protoplasts survival or may indirectly affect the exocytosis rate since LatA affects all actin structures in the cell, including actin cables which are needed for the transport of exocytic vesicles (Lo Presti et al., 2012).

Actin dynamics during clathrin-mediated endocytosis in wild-type walled cells is robust over a wide range of chronic and acute changes in media osmolarity

Next, we wondered how the actin machinery adapts to different changes in osmotic pressure and membrane tension. To monitor actin dynamics during clathrin-mediated endocytosis, we imaged fission yeast cells expressing Fim1p-mEGFP (Figures 6A and 6B). Fimbrin is a bona fide marker for endocytosis in yeast since it has spatial and temporal co-localization with the classical endocytic marker End4p (the fission yeast homolog of mammalian Hip1R and budding yeast Sla2) during endocytosis (Figure 6 – Supplement 1A and 6 – Supplement 1B). Fimbrin's time of appearance, disappearance, peak number of molecules and spatial localization follows those of actin in wild-type cells and all mutants tested so far (Arasada et al., 2018; Berro and Pollard, 2014b; Chen and Pollard, 2013; Sirotkin et al., 2010). Fimbrin is the most abundant endocytic proteins that is fully functional when tagged with a fluorescent protein at either N- or C-terminal. Tagged fimbrin is a more robust marker for actin dynamics than tagged actin or actin-binding markers such as LifeAct or calponin-homology domains, because they require over-expression which is difficult to control precisely in fission yeast, and potentially creates artifacts (Courtemanche et al., 2016; Suarez et al., 2015). Fimbrin is also a central player in force production during CME in yeast (Ma and Berro, 2019, 2018; Picco et al., 2018; Planade et al., 2019). We optimized our imaging protocols, and improved tracking tools and temporal super-resolution alignment methods (Berro and Pollard, 2014a) to a) easily collect hundreds of endocytic events in an unbiased manner and b) achieve high reproducibility between different samples, fields of view and days of experiment (Figures 6C and 6 – Supplement 2A). These improvements in our quantitative microscopy protocol have allowed us to detect small differences between mutants or conditions that would be missed with previous methods. We confirmed that Fim1p accumulates at endocytic sites for about 10 seconds, and then disassembles while the vesicle diffuses away from the plasma membrane (Figures 6C and 6 – Supplement 2A) (Sirotkin et al., 2010; Skau et al., 2011). As a convention, the peak number of Fim1p molecules is set to time 0 s and corresponds to vesicle scission in intact wild-type cells (Berro and Pollard, 2014a, 2014b; Sirotkin et al., 2010).

For all tested osmolarities at steady state in walled wild-type cells, we observed no significant difference in the dynamics of fimbrin recruitment or disassembly, maximum molecule number or endocytic patch movements (Figure 6D). Our results indicate that wild-type walled cells have adaptation mechanisms for chronic exposure to a wide range of osmolarities, which allows them to perform CME in a highly reproducible manner.

We then tested the robustness of the endocytic actin machinery when cells experienced a hypotonic shock, which aimed to abruptly increase the tension of their plasma membrane. To observe the highest possible effect, we imaged cells grown at steady state in 1.2 M sorbitol and rapidly exchanged the media with a buffer free of sorbitol (Figures 6F and 6G), therefore performing an acute hypotonic shock of ΔC=-1.2 M. Despite the high hypotonic shock, which represents a ~3 MPa drop in pressure, CME proceeded quite similarly to steady state conditions (Figures 6G, 6 – Supplement 3). The maximum number of fimbrin proteins was the same before and after the hypotonic shock, but fimbrin assembly and disassembly were ~15% faster after the shock.

Eisosomes mitigate the response of the endocytic machinery to acute and chronic changes in media osmolarity

The robustness of the endocytic process under a wide range of chronic and acute exposure to different media osmolarity is consistent with our previous results showing that fission yeast cells rapidly regulate plasma membrane tension. To better understand the role of eisosomes and amplify the change in membrane tension after hypotonic shocks, we repeated our experiments in *pil1Δ* cells which lack eisosomes (Figure 6E).

Dynamics of Fim1p during CME for wild-type and *pil1Δ* walled cells at steady state in media free of sorbitol were identical (Figure 6 – Supplement 1C). However, at steady state in media with high sorbitol concentration, cells lacking eisosomes recruited slightly fewer fimbrin molecules to endocytic patches than wild-type cells (Figure 6E). The maximum number of Fim1p assembled at CME sites in *pil1Δ* cells in buffer containing 0.8 M and 1.2 M sorbitol was 10% and 17% lower, respectively. Within the first two minutes of an acute hypotonic shock from 1.2 M sorbitol to 0 M (ΔC=-1.2 M), the maximum number of Fim1p increased by 30%, while its timing was shortened by ~30% compared to steady-state (Figure 6H). Four minutes after the hypotonic shock, the dynamics of fimbrin stabilized at its steady state dynamics in 0 M sorbitol (Figures 6E and 6H). Overall, our data show that the endocytic actin machinery in cells lacking eisosomes is more sensitive to acute and chronic changes in media osmolarity than in wild-type cells, consistent with a role for eisosome in regulating membrane tension at endocytic sites.

CME in protoplasts is sensitive to chronic changes in osmolarity

Endocytosis in wild-type protoplasts at steady state in medium containing 0.4 or 0.8 M sorbitol was able to proceed normally by recruiting almost the same number of fimbrin molecules as in walled cells, but with a slightly longer timing (Figure 7 – Supplement 1B). In contrast, in medium with 1.2 M sorbitol, the timing of fimbrin recruitment was dramatically longer, and endocytosis failed to proceed normally, as reported by the virtually null speed of patches during the entire time fimbrin was present at the endocytic site (Figure 7 – Supplement 1B). Cells lacking eisosomes had very similar phenotypes but endocytosis started failing at 0.8 M sorbitol (Figure 7 – Supplement 1C).

At 0.25 M sorbitol, both wild-type and *pil1Δ* protoplasts were able to perform endocytosis but required a larger amount of Fim1p (Figures 7 – Supplements 1B and 7 – Supplements 1C). In these conditions, the eisosomes covered only half of the plasma membrane surface area they cover at 0.4M sorbitol (Figures 1B and 1C) and our data suggest the plasma membrane was under high tension (Figure 1G). This result indicates that during CME the actin machinery is able to adapt to mechanical cues by mechanisms that are independent of the cell wall.

For both wild-type and *pil1Δ* protoplasts in 0.4 M sorbitol, the temporal evolution of the number of fimbrin molecules and the speed of patches were close to the same metrics measured in walled cells in media without sorbitol (Figures 7 – Supplements

1B and 7 – Supplements 1C). These results suggest that the osmotic pressure at these concentrations, which are equivalent to a pressure of 1 MPa, is close to the naturally maintained turgor pressure of walled fission yeast cells, in good agreement with previous measurements (Minc et al., 2009). Therefore, to keep protoplasts in conditions close to walled cells, the steady state media used in our following experiments on protoplasts contained 0.4 M sorbitol.

The endocytic actin machinery rapidly adapts to increases in membrane tension

To characterize the adaptation of the endocytic actin machinery to a rapid increase in turgor pressure and membrane tension, we repeated our acute hypotonic shocks (ΔC=-0.05 M, -0.1 M or -0.2 M) on protoplasts initially at steady state in media containing 0.4 M sorbitol. After low (ΔC=-0.05 M) and medium (ΔC=-0.1 M) acute shocks in wild-type protoplasts, we did not observe any stalled endocytic events – when cells started the recruitment of the actin machinery, endocytosis proceeded to successful completion (Figures 7A-C and 7 – Supplement 5). The recruitment of fimbrin did not significantly change over time. In contrast, two minutes after a ΔC=-0.2 M shock, endocytic sites recruited 20% more fimbrin and it took ~25% longer to perform endocytosis (Figures 7C, 7D, and 7 – Supplement 5). The actin machinery restored its steady state behavior less than 4 minutes after the shock (Figure 7D).

We repeated these experiments with *pil1Δ* protoplasts to eliminate the role of eisosomes in the reduction of membrane tension during hypotonic shocks. Immediately (0 minute) after the lowest hypotonic shock tested (ΔC=-0.05 M), fimbrin recruitment took slightly longer and the number of proteins recruited was higher than at steady state (Figures 7E-G and 7 – Supplement 6). While fimbrin restored its steady-state dynamics in less than 4 minutes after high acute hypotonic shock (ΔC=-0.2 M) in wild-type protoplasts (Figure 7D), recovery of fimbrin dynamics to its steady state behavior in *pil1Δ* protoplasts occurred over 10 minutes, even for the most modest hypotonic shock, ΔC=-0.05 M (Figure 7G). The changes in fimbrin dynamics in *pil1Δ* protoplasts became increasingly larger for ΔC=-0.1 M and ΔC=-0.2 M hypotonic shocks – endocytic sites assembled a peak number of fimbrin respectively ~25% and ~50% larger and took ~85% and ~50% longer.

Wild-type protoplasts at steady state in 0.25 M sorbitol contain significantly fewer assembled eisosomes despite expressing normal amounts of Pil1p (Figures 1B, 1C and 1E). We took advantage of this condition to test whether the absence of eisosomes structures at the plasma membrane and not the absence of the protein Pil1p is responsible for changes in actin dynamics after an acute hypotonic shock. We subjected wild-type protoplasts at steady state in 0.25 M sorbitol to an acute hypotonic shock of ΔC=-0.1 M (Figures 7H and 7I). Two minutes after the shock, endocytic sites accumulated 73% more fimbrin and took ~60% longer (Figures 7H and 7 – Supplement 7A). This behavior was nearly identical to fimbrin dynamics in *pil1Δ* protoplasts under the same conditions (Figure 7I and Figure 7 – Supplement 7B).

Altogether, these experiments demonstrate that a) the endocytic actin machinery adapts to compensate the increase in membrane tension, and b) actin dynamics restores its steady state behavior within a few minutes, providing the protoplasts survived the hypotonic shock.

Discussion

Mechanisms of tension regulation and homeostasis of the plasma membrane

Our results demonstrate that the regulation of membrane tension in hypotonic environment is performed via a combination of at least three mechanisms: the mechanical protection by the cell wall, the disassembly of eisosomes and the temporary shift in the balance between endocytosis and exocytosis (Figure 8). Our data indicate that all three mechanisms are used in parallel, since wild-type walled cells are less sensitive to acute hypotonic shocks than wild-type protoplasts and *pil1Δ* walled cells, and they experience a temporary decrease in their endocytic density for about 2 minutes after the shock. In addition, our data allow us to estimate the relative contribution of each mechanism in the regulation of membrane tension.

The cell wall provides the largest protection during chronic and acute hypotonic shocks. Wild-type walled cells are virtually insensitive to osmotic downshifts, and *pil1Δ* walled cells are much less sensitive than *pil1Δ* protoplasts. Removal of the cell wall dramatically affects actin dynamics at endocytic sites and eisosome assembly at the plasma membrane (Figures 1B, 1C, 7 – Supplement 1B and 7 – Supplement 1C), and greatly increased the effect of hypotonic shock on exocytosis (Figure 4). It is surprising that endocytosis in protoplasts still proceeds in media with osmolarity as low as 0.25 M, where a large fraction of eisosomes is disassembled. In fact, the actin endocytic machinery can overcome membrane tensions high enough to rupture the plasma membrane since we did not see stalled actin patches, or actin comet tails, in any of our experiments. Our results contrast with recent data in *S. cerevisiae* (Riggi et al., 2019) where endocytosis is blocked and actin comet tails are formed within 2 minutes of a hypotonic shock. These differences may highlight species specificities.

Our results add to a growing body of evidence that eisosomes play a critical role in the regulation of membrane tension and membrane integrity through dynamic remodeling and scaffolding of the plasma membrane (Kabeche et al., 2015; Moseley, 2018). Endocytosis in wild-type walled cells is not sensitive to chronic or acute hypotonic changes, whereas *pil1Δ* walled cells endocytosis is (Figure 6). Conversely, exocytosis seems to respond more strongly to acute hypotonic shock in wild-type walled cells than in *pil1Δ* walled cells (Figure 4). The protective role of eisosomes is even more striking in protoplasts under acute hypotonic shocks. Wild-type protoplasts whose plasma membrane is covered with eisosomes are largely insensitive to increases in membrane tension whereas protoplasts with little to no eisosomes are extremely sensitive to increases in membrane tension and their plasma membrane is easily damaged (Figures 2A-C). Eisosomes retain this protective function even in walled cells, which becomes evident when cells are put under repeated osmolarity shocks (Figures 2E-G). Our micropipette aspiration experiments also demonstrate that eisosomes are critical to keep membrane tension low during an acute hypotonic shock. Therefore, our data indicate that membrane tension is decreased via the disassembly of eisosomes, through release of excess membrane surface area. Assuming eisosomes are hemi-cylinders with diameter ~50 nm and cells contain 1.6 μm of eisosomes per μm^2 of plasma membrane on average, total eisosome disassembly could release about 5% of the total surface area of the plasma membrane over ~3 minutes after a hypotonic shock (Kabeche et al., 2015), although a mild shock of ΔC=-0.2 M disassembled close to ~50% eisosomes over 5 minutes, or about 2.5% of the surface area of the plasma membrane (Figures 1H and 1I). Single-molecule imaging in our lab demonstrated that at steady state Pil1p undergoes rapid exchange at the eisosome ends (Lacy et al., 2017), potentially providing a convenient route for rapid eisosome disassembly, analogous to filament depolymerization, in combination with eisosome breaking. Disassembled eisosome components have altered phosphorylation level or sub-cellular localization, which potentially relays the signaling from eisosome integrity to endocytosis and/or exocytosis (Riggi et al., 2018; Walther et al., 2007), possibly via TORC2 (Riggi et al., 2019).

Our study highlights a third mechanism to reduce membrane tension by increasing the surface area of the plasma membrane via a temporary reduction in the endocytosis rate and an increase in the exocytosis rate. Using our data, we estimate that cells endocytose about 2% of their surface area per minute through clathrin mediated endocytosis, confirming our previous measurements (Berro and Pollard, 2014a, 2014b). During acute hypotonic shock, a reduction of the endocytosis rate plus an increase in the exocytosis rate for a few minutes would allow for a net addition of surface area to the plasma membrane. For example, in *pil1Δ* protoplasts initially at steady state in 0.4 M sorbitol the endocytosis rate is reduced by ~25 % for ~10 minutes after an acute hypotonic shock of ΔC=-0.05 M, while the exocytosis rate increased by ~10%. The net surface area added over that period by reduction in endocytosis and increase in exocytosis corresponds to a 5% + 6% =11% increase in the protoplast surface area, close to the ~12% surface area increase we measured. These results confirm and quantify previous reports of control of surface tension by increasing the surface area via a modulation of endocytosis and exocytosis rates in other eukaryotes (Apodaca, 2002; Homann, 1998; Morris and Homann, 2001). These estimates demonstrate that modulating the endocytosis and exocytosis rates is an efficient way to increase the surface area of the plasma membrane by large amounts, but this process is relatively slow compared to eisosome disassembly. The slowness of this process might explain why *pil1Δ* and pre-stretched wild-type protoplasts that have about half the normal amount of eisosomes on their surface do not survive even relatively small hypotonic shocks, being unable to provide enough membrane in a short amount of time to reduce the tension of their plasma membrane.

For the calculations presented above, we have assumed that the size of endocytic and exocytic vesicles remain constant in all osmotic conditions. However, further experiments will be necessary to validate or invalidate this assumption. In addition, our FM4-64 data does not allow us to distinguish between lipid addition to the plasma membrane via exocytosis or via a putative transfer of lipids by non-exocytic mechanisms (Reinisch and Prinz, 2021) and for simplicity and by lack of further evidence, we have discussed our data as an increase in the exocytosis rate. Not much is known about lipid transfer proteins at the plasma membrane and further experiments will be necessary to determine whether the activity of these proteins is enhanced by abrupt increases in membrane tension or hypotonic shocks.

Molecular mechanisms driving the adaptation of the actin endocytic machinery and the rate of endocytosis under various membrane tensions

Our data demonstrate that fission yeast CME is very robust and can proceed in a wide range of osmolarities and membrane tension. Even cells devoid of a cell wall and eisosomes were able to perform endocytosis after an acute change in membrane tension, as long as their plasma membrane was not damaged and cells remained alive. Even in the most extreme conditions tested, i.e. cells devoid of a cell wall and lacking the majority of their eisosomes, the peak number of molecules and timing of fimbrin at endocytic sites was only two times larger than what was observed in wild-type walled cells.

Under conditions where membrane tension and turgor pressure were significantly increased, we observed that the endocytic actin machinery took longer and assembled a larger number of fimbrin molecules to successfully produce endocytic vesicles. This effect increased with increasing membrane tension, up to tensions high enough to rupture the cell plasma membrane. This result strongly supports the idea that the actin machinery provides the force that counteracts membrane tension and turgor pressure and deforms the plasma membrane into an endocytic pit.

The precise molecular mechanism that regulates this enhanced assembly remains to be uncovered. Our data suggest that actin dynamics is controlled via a mechanical or geometrical regulation, where actin assembles until the plasma membrane is deformed and pinched off. An alternative, and non-mutually exclusive, hypothesis is that the activity and/or recruitment of proteins upstream of the actin nucleators may be enhanced by increased membrane tension. A third hypothesis is that the decrease in the number of endocytic events after an increase in membrane tension leads to an increase in the concentration of endocytic proteins in the cytoplasm, which can then enhance the reactions performed at the endocytic sites. Sirotkin et al (Sirotkin et al., 2010) measured that 65% to 85% of the total cellular content of key proteins involved in the endocytic actin machinery are localized to endocytic sites at any time. A 20% decrease in the number of endocytic sites would increase their cytoplasmic abundance by roughly 40% to 80%. This percentage is larger than the volume changes we measured, resulting in a net increase in the cytoplasmic concentration of these proteins, which would allow larger amount of protein to assemble at the endocytic sites.

Conversely, the decreased endocytosis rate could be attributed to the larger number of endocytic proteins assembled at each endocytic site, which would decrease their cytoplasmic concentration. Indeed, Burke *et al*. (Burke et al., 2014) showed that modulating actin concentration modulates the number of endocytic sites in the same direction. However, it is more likely that one or several early endocytic proteins are sensitive to membrane tension, and either fail to bind the plasma membrane or prevent the triggering of actin assembly when membrane tension is high. This idea would be consistent with results from mammalian cells demonstrating that the proportion of stalled clathrin-coated pits increases when membrane tension increases (Ferguson et al., 2017). In addition, several endocytic proteins that arrive before or concomitantly with the activators of the actin machinery contain BAR domains (such as Syp1p, Bzz1p and Cdc15p), and other members of this domain family (which also includes Pil1p) have been shown to bind membranes in a tension-sensitive manner. Further quantitative study of early endocytic proteins will help uncover the validity and relative contributions of each one of these hypotheses.

We expect our results to be relevant to the study of CME and membrane tension regulation in other eukaryotes since the molecular machineries for endocytosis, exocytosis and osmotic response are highly conserved. In addition, regulation of membrane tension and CME are particularly critical during cell polarization (Mostov et al., 2000), during neuron development and shape changes (Urbina et al., 2018) and at synapses where large pools of membranes are added and retrieved on a very fast time scale (Nicholson-Fish et al., 2016; Watanabe and Boucrot, 2017).

Materials and Methods

Key Resources Table

Reagent type (species) or resource	**Designation**	**Source or reference**	**Identifiers**	**Additional information**
Strain, strain background (*Schizosaccharomyces pombe*)	Fim1p-mEGFP	(Berro and Pollard, 2014a)	SpJB57	fim1-mEGFP-NatMX6 ade6-M216 his3-Δ1 leu1-32 ura4-Δ18 h+
Strain, strain background (*Schizosaccharomyces pombe*)	Pil1p-mEGFP	(Lacy et al., 2017)	SpJB204	pil1-mEGFP-kanMX6 ade6-M216 his3-Δ1 leu1-32 ura4-Δ18 h-
Strain, strain background (*Schizosaccharomyces pombe*)	*pil1Δ* Fim1p-mEGFP	This study	SpJB234	pil1Δ fim1-mEGFP-NatMX6 ade6-M216 his3-Δ1 leu1-32 ura4-Δ18 h-
Strain, strain background (*Schizosaccharomyces pombe*)	mScarlet-I-End4p mEGFP-Fim1p	This study	SpJB566	mScarlet-I-end4 mEGFP-fim1 fex1Δ fex2Δ ade6-M216 his3-D1 leu1-32 ura4-D18 h-
Chemical compound, drug	FM4-64	Biotium, Fremont, CA, USA		

Chemical compound, drug	sulforhodamine B	MP Biomedicals LLC, Santa Ana, USA		
Chemical compound, drug	Latrunculin A	Millipore, MA, USA		
Chemical compound, drug	Brefeldin A	Santa Cruz Biotechnology Inc., TX, USA		
Software, algorithm	Matlab	Mathworks	R2016a	
Software, algorithm	FIJI ImageJ	(Schindelin et al., 2012; Schneider et al., 2012)		
Software, algorithm	Trackmate	(Tinevez et al., 2017)		
Software, algorithm	PatchTrackingTools	This study	Version 2015.12.16	https://bitbucket.org/jberro/patchtrackingtools/src/stable/
Software, algorithm	PatchTrackingDataPostprocessing.Deterministic	This study	Version 160801	https://bitbucket.org/jberro/patchtrackingdatapostprocessing.deterministic/src/master/

Yeast strains and media

The *S. pombe* strains used in this study are listed in the Key Resources Table. Yeast cells were grown in YE5S (Yeast Extract supplemented with 0.225 g/L of uracil, lysine, histidine, adenine and leucine), which was supplemented with 0 to 1.2 M D-Sorbitol, at 32°C in exponential phase for about 18 hours. Cells were washed twice and resuspended in filtered EMM5S (Edinburgh Minimum media supplemented with 0.225 g/L of uracil, lysine, histidine, adenine and leucine), which was supplemented with the same concentration of D-Sorbitol, at least 10 minutes before imaging so they can adapt and reach steady state.

Protoplasts preparation

S. pombe cells were grown in YE5S at 32°C in exponential phase for about 18 hours. 10 mL of cells were harvested and washed two times with SCS buffer (20 mM citrate buffer, 1 M D-Sorbitol, pH=5.8), and resuspended in SCS supplemented with 0.1 g/mL Lallzyme (Lallemand, Montreal, Canada) (Flor-Parra et al., 2014). Cells were incubated with gentle shaking for 10 minutes at 37°C in the dark except for experiments in Figure 5, where cells were digested at room temperature with gentle shaking for 30 minutes in the presence of inhibitors. The resulting protoplasts were gently washed twice in EMM5S with 0.25 to 1.2 M D-Sorbitol, spun down for 3 minutes at 960 rcf between washes, and resuspended in EMM5S buffer supplemented with 0.25 to 1.2 M D-Sorbitol at least 10 minutes before imaging so they can adapt and reach steady state.

Microscopy

Microscopy was performed using a spinning disk confocal microscope, built on a TiE inverted microscope (Nikon, Tokyo, Japan), equipped with a CSU-W1 spinning head (Yokogawa Electric Corporation, Tokyo, Japan), a 100X/1.45NA Phase objective, an iXon Ultra888 EMCCD camera (Andor, Belfast, UK), and the NIS-Elements software v. 4.30.02 (Nikon, Tokyo, Japan) on. The full system was switched on at least 45 minutes prior to any experiments to stabilize the laser power and the room temperature. Cells were loaded into commercially available microfluidics chambers for haploid yeast cells (Y04C-02-5PK, Millipore-Sigma, Saint-Louis, USA) for the CellASIC ONIX2 microfluidics system (Millipore-Sigma, Saint-Louis, USA). Each field of view was imaged for 60 seconds, and each second a stack of 6 z-slices separated by 0.5 µm was imaged. The microscope was focused such that the part of the cell closest to the coverslip was captured.

Acute hypotonic shocks

Walled cells or protoplasts were first imaged in their steady state media (EMM5S supplemented with 0 to 1.2 M D-Sorbitol). The steady state media was exchanged with media supplemented with a lower D-Sorbitol concentration (the concentration difference is noted ΔC), with inlet pressure of 5 psi. This hypotonic shock media was labelled with 6.7 µg/mL of sulforhodamine B (MP Biomedicals LLC, Santa Ana, USA), a red cell-impermeable dye that allowed us to a) monitor the full exchange of the solution in the microfluidic chamber prior to image acquisition, and b) monitor the plasma membrane integrity of the cells after the shock. In each condition, the first movie was started when the sulforhodamine B dye was visible in the field of view. For clarity, this time point is labelled t=0 min in all our figures, but note that we estimate it may vary by up to ~30 seconds between movies and conditions. We imaged cells by taking one stack of 6 Z-slices per second for 60 seconds. After the end of each movie, we rapidly changed field of view and restarted acquisition one minute after the end of the previous movie, so that movies started every 2 minutes after the acute hypotonic shock. Tracks from cells that contained red fluorescence from the sulforhodamine B dye were excluded from the analysis, because this indicated that cell membrane had been damaged.

Inhibition of endocytosis and exocytosis during acute hypotonic shock

Endocytosis or exocytosis was inhibited by including respectively 25uM Latrunculin A (Millipore, MA, USA) or 2mM Brefeldin A (Santa Cruz Biotechnology Inc., TX, USA) in the solution used to prepare the protoplasts and and to perform the hypotonic shocks. Hypotonic shock solution also included 20 µM FM4-64 (Biotium, Fremont, CA, USA) to stain dead protoplasts (Vida and Gerhardt, 1999) (Figure 5A), and inlet pressure was set at 4 psi.

Measurement of the temporal evolution of the number of proteins and speed

Movies were processed and analyzed using an updated version of the PatchTrackingTools toolset for the Fiji (Schindelin et al., 2012) distribution of ImageJ (Berro and Pollard, 2014a; Schneider et al., 2012). This new version includes automatic patch tracking capabilities based on the Trackmate library (Tinevez et al., 2017), and is available on the Berro lab website: http://campuspress.yale.edu/berrolab/ publications/software/ and the lab bitbucket https://bitbucket.org/jberro/. Prior to any quantitative measurements, we corrected our movies for uneven illumination and camera noise. The uneven illumination was measured by imaging a solution of Alexa 488 dye and the camera noise was measured by imaging a field of view with 0% laser power. We tracked Fim1-mEGFP spots with a circular 7-pixel diameter region of interest (ROI), and measured the temporal evolution of the fluorescence intensities and the position of the centers of mass. The spot intensity was corrected for cytoplasmic background using a 9-pixel median filter, and was then corrected for photobleaching. The photobleaching rate was estimated by fitting a single exponential to the temporal evolution of the intensity of cytoplasmic ROIs void of any identifiable spots of fluorescence (Berro and Pollard, 2014a). Only tracks longer than 5 s and displaying an increase followed by a decrease in intensity were kept for the analysis. Individual tracks were aligned and averaged with the temporal super-resolution algorithm from (Berro and Pollard, 2014a), and post-processed to generate figures using the Matlab R2016a (Mathworks) scripts PatchTrackingDataPostprocessing.Deterministic, available on the Berro lab website: http://campuspress.yale.edu/berrolab/ publications/software/ and the lab bitbucket https://bitbucket.org/jberro/ . In brief, this method realigns temporal signals that have low temporal resolution and where no absolute time reference is available to align them relatively to each other. It iteratively finds the temporal offset which has a higher precision than the measured signal and minimizes the mean square difference between each measured signal and a reference signal. For the first round of alignments, the reference signal is one of the measurements. After each realignment round, a new reference is calculated as the mean of all the realigned signals, which is an estimator of the true underlying signal.

To control and calibrate the intensity of our measurements, we imaged wild-type walled cell expressing Fim1p-mEGP each imaging day. Intensities were converted into number of molecules with a calibration factor such that the peak intensity of our control strain corresponded to 830 molecules (Berro and Pollard, 2014a).

In all figures presenting the temporal evolution of the number of molecules or the speed, time 0 s corresponds to the time point when the number of molecules is maximum (also called the peak number). The "speed vs time" plots helps determine whether endocytosis completes normally in different conditions. At a given time point, the speed corresponds to the average movement of the endocytic structure in the plane of the membrane between two consecutive images. For an endocytic event that completes normally, the speed is close to 0 while the endocytic pit elongates before the vesicle is pinched off. Note that the speed is not exactly 0 because of localization errors and putative small movements of the endocytic structure in the plane of the membrane. The speed increases after the vesicle is pinched off and it diffuses freely in the cytoplasm. Since this movement is mostly diffusive, the standard deviations of the speeds are large.

Satistical tests between conditions were performed at time 0 s with a one-way ANOVA test using the number of tracks collected to build the figure. To avoid extrapolating the data, we compared the relative duration of assembly and disassembly between conditions using the time at which the average number of molecules reach half the peak number.

Measurement of the density of CME events

We used the *S. Pombe* profiling tools for ImageJ (Berro and Pollard, 2014a) to measure the number of endocytic events at a given time in each cell. In brief, on a sum-projected z-stack, we manually outlined individual cells, and, for each position along the long axis of a cell, we measured the sum of fluorescence orthogonal to the long axis. We corrected the intensity profile in each cell for its cytoplasmic intensity and media fluorescence outside the cell. We estimated the number of patches in each cell by dividing the corrected fluorescence signal with the temporal average of the fluorescence intensity of one endocytic event. We calculated the linear density of endocytic events as the ratio between the number of endocytic events in a cell and its length.

We estimated the percentage of plasma membrane internalized by endocytosis per minute as follows. We measured ~120 endocytic sites per cell at a given time on average. Since the actin meshwork assembles and disassembles in about 20 seconds, we estimate that 360 endocytic vesicles are formed per minute. Assuming endocytic vesicles have a 50-nm diameter, this corresponds to a ~2.8 μm^2 endocytosed per minute, or ~2% of the total surface area, considering the average cell is around 12 µm long and has a 132 μm^2 of plasma membrane (assuming the cell shape is a cylinder capped by two hemispheres).

Measurement of the exocytosis rate with FM4-64 staining

The exocytosis rate was measured by combining the acute hypotonic shock with FM4-64 staining, in a similar approach as has been reported (Gauthier et al., 2009; Smith and Betz, 1996; Vida and Emr, 1995). The cell impermeable dye FM4-64 (Biotium, Fremont, CA, USA) was diluted to a final concentration of 20 µM in any of the media used. When cells are exposed to FM4-64, the dye rapidly stains the outer leaflet of the plasma membrane. Upon endocytosis, the dye is trafficked inside the cell without change in fluorescence. The total cell fluorescence intensity was measured after segmenting the cells by thresholding the fluorescence signal above background levels. The fluorescence intensity was normalized to the intensity reached at the end of the fast increase ~1 min after the dye was flowed in, which corresponds to the intensity of total surface area of the plasma membrane (Figure

4B). After this fast phase (< 20 seconds), the fluorescence signal increased more slowly every time unstained membrane was exposed to the cell surface by exocytosis. At short time scale (~5 to 20 min depending on the exocytosis rate), recycling of stained membrane is negligible and one can assume that all exocytosed membrane is virtually unstained. Since the intensity at the beginning of the slow phase was normalized to 1, the slope of the linear increase of fluorescence is equal to the amount of membrane exocytosed per minute, expressed as a fraction of the surface area of the plasma membrane. For all measurements, images were taken at 5 s interval at the middle plane of cells with the help of Perfect Focusing System (Nikon, Tokyo, Japan), with minimal laser excitation in order to reduce toxicity and photobleaching to negligible values. Curve fitting and slope calculation was performed in GraphPad Prism (GraphPad Software, La Jolla, CA, USA).

Measurement of eisosomes' density on the plasma membrane

We imaged full cells expressing Pil1p-mEGFP by taking stacks of 0.5 µm spaced Z-slices. We corrected these Z-stacks for uneven illumination and manually outlined individual cells to determine the surface area of each cell. To determine the total amount of eisosome-bound Pil1p-mEGFP we subtracted the cytosolic intensity of Pil1-mEGFP using a pre-determined threshold and summed all the Z-slices. We measured the mean membrane intensity of each cell on the thresholded sum-projection image. The eisosome density was determined by dividing this mean intensity by the surface area of each protoplast.

To quantify the relative changes in area fraction of eisosomes after acute hypotonic shock, wild-type protoplasts expressing Pil1p-mEGFP were loaded into ONIX2 microfluidics system (Millipore-Sigma, Saint-Louis, USA), and time-lapse fluorescent images were taken at a single Z-slice at the top of protoplasts during media change. After background correction, the total area fraction of eisosomes at the beginning of hypotonic shock was set to 1.0 for normalization, and the normalized values of area fraction were fit to a single exponential decay curve in GraphPad Prism (GraphPad Software, La Jolla, CA, USA).

Measurement of membrane tension

Protoplasts were loaded in a custom-built chamber which was passivated with 0.2 mg/mL β-casein (Millipore-Sigma, Saint-Louis, USA) for 30 minutes and pre-equilibrated with EMM5S supplemented with 0.8 M D-Sorbitol. A glass micropipette (#1B100-4, World Precision Instruments, Sarasota, USA) was forged to a diameter smaller than the average protoplast radius (~2.5 µm), and was connected to a water reservoir of adjustable height to apply a defined aspiration pressure. Before and after each experiment the height of the water reservoir was adjusted to set the aspiration pressure to 0. Cells were imaged with a bright field IX-71 inverted microscope (Olympus, Tokyo, Japan) equipped with a 60X/1.4NA objective, and images were recorded every second. Aspiration pressure was gradually increased every 30 s and the membrane tension σ was calculated as $\sigma = \Delta P . R_p/[2(1 - R_p/R_c)]$, where R_p and R_c are respectively the micropipette and the cell radius, ΔP is the aspiration pressure for which the length of the tongue l of the protoplast in the micropipette is equal to R_p (Evans and Yeung, 1989). To limit the effects of the adaptation of cells' membrane tension, all measurements were performed within the first five minutes after the hypotonic shock, which greatly limited the throughput of our assay (1 measurement per sample), compared to the measurements at steady state (around 6 measurements per sample).

Acknowledgements

We thank Yale West Campus Imaging core for providing access to the spinning disc confocal microscope, members of the Berro lab for insightful discussions and R. Fernandez for providing mutant yeast strains. We thank Ramesh Ramji and Kathryn Miller-Jensen for initial help with the microfluidics part of this project. We gratefully thank Millipore Sigma for lending us a CellASIC unit and Erdem Karatekin for access to his micropipette aspiration setup. We also thank Samantha Dundon, Mike Lacy and Matt Akamatsu for their comments on our manuscript. This research was supported in part by National Institutes of Health/National Institute of General Medical Sciences Grant R01GM115636 and by seed funding from the American Cancer Society Institutional Research Grant #IRG 58-012-58.

References

Aghamohammadzadeh S, Ayscough KR. 2009. Differential requirements for actin during yeast and mammalian endocytosis. *Nature cell biology* **11**:1039–1042. doi:10.1038/ncb1918

Aghamohammadzadeh S, Smaczynska-de Rooij II, Ayscough KR. 2014. An Abp1-dependent route of endocytosis functions when the classical endocytic pathway in yeast is inhibited. *PLoS ONE* **9**. doi:10.1371/journal.pone.0103311

Apodaca G. 2002. Modulation of membrane traffic by mechanical stimuli. *American Journal of Physiology-Renal Physiology* **282**:F179–F190. doi:10.1152/ajprenal.2002.282.2.F179

Arasada R, Pollard TD. 2011. Distinct Roles for F-BAR Proteins Cdc15p and Bzz1p in Actin Polymerization at Sites of Endocytosis in Fission Yeast. *Current Biology* **21**:1450–1459. doi:10.1016/j.cub.2011.07.046

Arasada R, Sayyad WAWA, Berro J, Pollard TDTD. 2018. High-speed superresolution imaging of the proteins in fission yeast clathrin-mediated endocytic actin patches. *Molecular Biology of the Cell* **29**:295–303. doi:10.1091/mbc.E17-06-0415

Atilgan E, Magidson V, Khodjakov A, Chang F. 2015. Morphogenesis of the Fission Yeast Cell through Cell Wall Expansion. *Current biology : CB* **25**:2150–7. doi:10.1016/j.cub.2015.06.059

Basu R, Munteanu EL, Chang F. 2013. Role of turgor pressure in endocytosis in fission yeast. *Molecular biology of the cell* **25**:679–87. doi:10.1091/mbc.E13-10-0618

Berro J, Lacy MM. 2018. Quantitative Biology of Endocytosis, Colloquium Series on Quantitative Cell Biology (Marshall WF, ed). San Rafael (CA): Morgan & Claypool.

Berro J, Pollard TD. 2014a. Local and global analysis of endocytic patch dynamics in fission yeast using a new “temporal superresolution” realignment method. *MBoC* **25**:3501–3514. doi:10.1091/mbc.E13-01-0004

Berro J, Pollard TD. 2014b. Synergies between Aip1p and capping protein subunits (Acp1p and Acp2p) in clathrin-mediated endocytosis and cell polarization in fission yeast. *MBoC* **25**:3515–3527. doi:10.1091/mbc.E13-01-0005

Berro J, Pollard TD. 2014c. Local and global analysis of endocytic patch dynamics in fission yeast using a new “temporal superresolution” realignment method. *Molecular biology of the cell* **25**:3501–14. doi:10.1091/mbc.E13-01-0004

Berro J, Sirotkin V, Pollard TD. 2010. Mathematical modeling of endocytic actin patch kinetics in fission yeast: disassembly requires release of actin filament fragments. *MBoC* **21**:2905–2915. doi:10.1091/mbc.E10-06-0494

Boulant S, Kural C, Zeeh J-C, Ubelmann F, Kirchhausen T. 2011. Actin dynamics counteract membrane tension during clathrin-mediated endocytosis. *Nature cell biology* **13**:1124–1131. doi:10.1038/ncb2307

Burke TA, Christensen JR, Barone E, Suarez C, Sirotkin V, Kovar DR. 2014. Homeostatic actin cytoskeleton networks are regulated by assembly factor competition for monomers. *Current Biology* **24**:579–585. doi:10.1016/j.cub.2014.01.072

Carlsson AE, Bayly P V. 2014. Force generation by endocytic actin patches in budding yeast. *Biophysical Journal* **106**:1596–1606. doi:10.1016/j.bpj.2014.02.035

Chen Q, Pollard TD. 2013. Actin Filament Severing by Cofilin Dismantles Actin Patches and Produces Mother Filaments for New Patches. *Current Biology* **23**:1154–1162. doi:10.1016/J.CUB.2013.05.005

Cheng JPX, Mendoza-Topaz C, Howard G, Chadwick J, Shvets E, Cowburn AS, Dunmore BJ, Crosby A, Morrell NW, Nichols BJ. 2015. Caveolae protect endothelial cells from membrane rupture during increased cardiac output. *The Journal of Cell Biology* **211**:53–61. doi:10.1083/jcb.201504042

Cochilla AJ, Angleson JK, Betz WJ. 1999. MONITORING SECRETORY MEMBRANE WITH FM1-43 FLUORESCENCE. *Annual Review of Neuroscience* **22**:1–10. doi:10.1146/annurev.neuro.22.1.1

Courtemanche N, Pollard TD, Chen Q. 2016. Avoiding artefacts when counting polymerized actin in live cells with LifeAct fused to fluorescent proteins. *Nature Cell Biology* **18**:676–683. doi:10.1038/ncb3351

Davì V, Tanimoto H, Ershov D, Haupt A, De Belly H, Le Borgne R, Couturier E, Boudaoud A, Minc N. 2018. Mechanosensation Dynamically Coordinates Polar Growth and Cell Wall Assembly to Promote Cell Survival. *Developmental cell* **45**:170-182.e7. doi:10.1016/j.devcel.2018.03.022

Dmitrieff S, Nédélec F. 2015. Membrane Mechanics of Endocytosis in Cells with Turgor. *PLoS Computational Biology* **11**. doi:10.1371/journal.pcbi.1004538

Evans E, Yeung a. 1989. Apparent viscosity and cortical tension of blood granulocytes determined by micropipet aspiration. *Biophysical journal* **56**:151–160. doi:10.1016/S0006-3495(89)82660-8

Ferguson JP, Huber SD, Willy NM, Aygün E, Goker S, Atabey T, Kural C. 2017. Mechanoregulation of clathrin-mediated endocytosis. *Journal of Cell Science* **130**:3631–3636. doi:10.1242/jcs.205930

Ferguson S, Raimondi A, Paradise S, Shen H, Mesaki K, Ferguson A, Destaing O, Ko G, Takasaki J, Cremona O, O' Toole E, De Camilli P. 2009. Coordinated Actions of Actin and BAR Proteins Upstream of Dynamin at Endocytic Clathrin-Coated Pits. *Developmental Cell* **17**:811–822. doi:10.1016/j.devcel.2009.11.005

Flor-Parra I, Zhurinsky J, Bernal M, Gallardo P, Daga RR. 2014. A Lallzyme MMX-based rapid method for fission yeast protoplast preparation. *Yeast* **31**:61–66. doi:10.1002/yea.2994

Gachet Y, Hyams JS. 2005. Endocytosis in fission yeast is spatially associated with the actin cytoskeleton during polarised cell growth and cytokinesis. *Journal of Cell Science* **118**:4231–4242. doi:10.1242/jcs.02530

Gauthier NC, Rossier OM, Mathur A, Hone JC, Sheetz MP. 2009. Plasma Membrane Area Increases with Spread Area by Exocytosis of a GPI-anchored Protein Compartment. *Molecular Biology of the Cell* **20**:3261–3272. doi:10.1091/mbc.e09-01-0071

Goode BL, Eskin JA, Wendland B. 2015. Actin and endocytosis in budding yeast. *Genetics* **199**:315–58. doi:10.1534/genetics.112.145540

Hassinger JE, Oster G, Drubin DG, Rangamani P. 2017. Design principles for robust vesiculation in clathrin-mediated endocytosis. *Proceedings of the National Academy of Sciences* **114**:E1118–E1127. doi:10.1073/pnas.1617705114

Homann U. 1998. Fusion and fission of plasma-membrane material accommodates for osmotically induced changes in the surface area of guard-cell protoplasts. *Planta* **206**:329–333. doi:10.1007/s004250050408

Kabeche R, Howard L, Moseley JB. 2015. Eisosomes provide membrane reservoirs for rapid expansion of the yeast plasma membrane. *Journal of Cell Science* **128**:4057–4062. doi:10.1242/jcs.176867

Lacy MM, Baddeley D, Berro J. 2019. Single-molecule turnover dynamics of actin and membrane coat proteins in clathrin-mediated endocytosis. *eLife* **8**:e52355. doi:10.7554/elife.52355

Lacy MM, Baddeley D, Berro J. 2017. Single-molecule imaging of the BAR-domain protein Pil1p reveals filament-end dynamics. *MBoC* **28**:2251–2259. doi:10.1091/mbc.e17-04-0238

Lacy MM, Ma R, Ravindra NG, Berro J. 2018. Molecular mechanisms of force production in clathrin-mediated endocytosis. *FEBS Letters* **592**:3586–3605. doi:10.1002/1873-3468.13192

Lo HP, Hall TE, Parton RG. 2016. Mechanoprotection by skeletal muscle caveolae. *BioArchitecture* **0992**:00–00. doi:10.1080/19490992.2015.1131891

Lo Presti L, Chang F, Martin SG. 2012. Myosin Vs organize actin cables in fission yeast. *Molecular Biology of the Cell*. doi:10.1091/mbc.E12-07-0499

Ma R, Berro J. 2021. Endocytosis against high turgor pressure is made easier by partial protein coating and a freely rotating base. *Biophysical Journal*. doi:10.1016/j.bpj.2021.02.033

Ma R, Berro J. 2019. Crosslinking actin networks produces compressive force. *Cytoskeleton* **76**:346–354. doi:10.1002/cm.21552

Ma R, Berro J. 2018. Structural organization and energy storage in crosslinked actin assemblies. *PLOS Computational Biology* **14**:e1006150. doi:10.1371/journal.pcbi.1006150

Minc N, Boudaoud A, Chang F. 2009. Mechanical forces of fission yeast growth. *Current biology : CB* **19**:1096–1101. doi:10.1016/j.cub.2009.05.031

Morris CE, Homann U. 2001. Cell Surface Area Regulation and Membrane Tension. *The Journal of Membrane Biology* **179**:79–102. doi:10.1007/s002320010040

Moseley JB. 2018. Eisosomes. *Current Biology* **28**:R376–R378. doi:10.1016/J.CUB.2017.11.073

Mostov KE, Verges M, Altschuler Y. 2000. Membrane traffic in polarized epithelial cells. *Current Opinion in Cell Biology* **12**:483–490. doi:10.1016/S0955-0674(00)00120-4

Nicholson-Fish JC, Smillie KJ, Cousin MA. 2016. Monitoring activity-dependent bulk endocytosis with the genetically-encoded reporter VAMP4-pHluorin. *Journal of Neuroscience Methods* **266**:1–10. doi:10.1016/j.jneumeth.2016.03.011

Palmer SE, Smaczynska-de Rooij II, Marklew CJ, Allwood EG, Mishra R, Johnson S, Goldberg MW, Ayscough KR. 2015. A dynamin-actin interaction is required for vesicle scission during endocytosis in yeast. *Current Biology* **25**:868–878. doi:10.1016/j.cub.2015.01.061

Parton RG, Pozo MA del, Vassilopoulos S, Nabi IR, Lay SL, Lundmark R, Kenworthy AK, Camus A, Blouin CM, Sessa WC, Lamaze C. 2019. Caveolae: The FAQs. *Traffic* **n/a**. doi:10.1111/tra.12689

Picco A, Kukulski W, Manenschijn HE, Specht T, Briggs JAG, Kaksonen M, Lemmon S. 2018. The contributions of the actin machinery to endocytic membrane bending and vesicle formation. *MBoC* **29**:1346–1358. doi:10.1091/mbc.E17-11-0688

Planade J, Belbahri R, Sanders MB, Guillotin A, Roure O du, Michelot A, Heuvingh J. 2019. Mechanical stiffness of reconstituted actin patches correlates tightly with endocytosis efficiency. *PLOS Biology* **17**:e3000500. doi:10.1371/journal.pbio.3000500

Reinisch KM, Prinz WA. 2021. Mechanisms of nonvesicular lipid transport. *Journal of Cell Biology* **220**. doi:10.1083/jcb.202012058

Richards DA, Guatimosim C, Betz WJ. 2000. Two Endocytic Recycling Routes Selectively Fill Two Vesicle Pools in Frog Motor Nerve Terminals. *Neuron* **27**:551–559. doi:10.1016/S0896-6273(00)00065-9

Riggi M, Bourgoint C, Macchione M, Matile S, Loewith R, Roux A. 2019. TORC2 controls endocytosis through plasma membrane tension. *The Journal of Cell Biology*. doi:10.1083/jcb.201901096

Riggi M, Niewola-Staszkowska K, Chiaruttini N, Colom A, Kusmider B, Mercier V, Soleimanpour S, Stahl M, Matile S, Roux A, Loewith R. 2018. Decrease in plasma membrane tension triggers PtdIns(4,5)P2 phase separation to inactivate TORC2. *Nature Cell Biology* **20**:1043–1051. doi:10.1038/s41556-018-0150-z

Schaber J, Adrover MÀ, Eriksson E, Pelet S, Petelenz-Kurdziel E, Klein D, Posas F, Goksör M, Peter M, Hohmann S, Klipp E. 2010. Biophysical properties of Saccharomyces cerevisiae and their relationship with HOG pathway activation. *European Biophysics Journal* **39**:1547–1556. doi:10.1007/s00249-010-0612-0

Schindelin J, Arganda-Carreras I, Frise E, Kaynig V, Longair M, Pietzsch T, Preibisch S, Rueden C, Saalfeld S, Schmid B, Tinevez JY, White DJ, Hartenstein V, Eliceiri K, Tomancak P, Cardona A. 2012. Fiji: An open-source platform for biological-image analysis. *Nature Methods*. doi:10.1038/nmeth.2019

Schneider CA, Rasband WS, Eliceiri KW. 2012. NIH Image to ImageJ: 25 years of image analysis. *Nature Methods* **9**:671–675. doi:10.1038/nmeth.2089

Sens P, Turner MS. 2006. Budded membrane microdomains as tension regulators. *Physical Review E - Statistical, Nonlinear, and Soft Matter Physics* **73**:1–4. doi:10.1103/PhysRevE.73.031918

Sinha B, Köster D, Ruez R, Gonnord P, Bastiani M, Abankwa D, Stan R V., Butler-Browne G, Vedie B, Johannes L, Morone N, Parton RG, Raposo G, Sens P, Lamaze C, Nassoy P. 2011. Cells respond to mechanical stress by rapid disassembly of caveolae. *Cell* **144**:402–413. doi:10.1016/j.cell.2010.12.031

Sirotkin V, Berro J, Macmillan K, Zhao L, Pollard TD. 2010. Quantitative analysis of the mechanism of endocytic actin patch assembly and disassembly in fission yeast. *Molecular biology of the cell* **21**:2894–904. doi:10.1091/mbc.E10-02-0157

Skau CT, Courson DS, Bestul AJ, Winkelman JD, Rock RS, Sirotkin V, Kovar DR. 2011. Actin filament bundling by fimbrin is important for endocytosis, cytokinesis, and polarization in fission yeast. *The Journal of biological chemistry* **286**:26964–77. doi:10.1074/jbc.M111.239004

Smith CB, Betz WJ. 1996. Simultaneous independent measurement of endocytosis and exocytosis. *Nature* **380**:531–534. doi:10.1038/380531a0

Stachowiak MR, Laplante C, Chin HF, Guirao B, Karatekin E, Pollard TD, O'Shaughnessy B. 2014. Mechanism of cytokinetic contractile ring constriction in fission yeast. *Developmental cell* **29**:547–61. doi:10.1016/j.devcel.2014.04.021

Suarez C, Carroll RT, Burke TA, Christensen JR, Bestul AJ, Sees JA, James ML, Sirotkin V, Kovar DR. 2015. Profilin Regulates F-Actin Network Homeostasis by Favoring Formin over Arp2/3 Complex. *Developmental Cell* **32**:43–53. doi:10.1016/J.DEVCEL.2014.10.027

Tinevez JY, Perry N, Schindelin J, Hoopes GM, Reynolds GD, Laplantine E, Bednarek SY, Shorte SL, Eliceiri KW. 2017. TrackMate: An open and extensible platform for single-particle tracking. *Methods* **115**:80–90. doi:10.1016/j.ymeth.2016.09.016

Urbina FL, Gomez SM, Gupton SL. 2018. Spatiotemporal organization of exocytosis emerges during neuronal shape change. *Journal of Cell Biology* **217**:1113–1128. doi:10.1083/jcb.201709064

Vida T, Gerhardt B. 1999. A Cell-Free Assay Allows Reconstitution of Vps33p-Dependent Transport to the Yeast Vacuole/Lysosome. *J Cell Biol* **146**:85–98.

Vida TA, Emr SD. 1995. A new vital stain for visualizing vacuolar membrane dynamics and endocytosis in yeast. *The Journal of cell biology* **128**:779–92. doi:10.1083/JCB.128.5.779

Walther TC, Aguilar PS, Fröhlich F, Chu F, Moreira K, Burlingame AL, Walter P. 2007. Pkh-kinases control eisosome assembly and organization. *The EMBO journal* **26**:4946–55. doi:10.1038/sj.emboj.7601933

Watanabe S, Boucrot E. 2017. Fast and ultrafast endocytosis. *Current Opinion in Cell Biology* **47**:64–71. doi:10.1016/j.ceb.2017.02.013

Figures

Figure 1: Eisosomes disassemble to buffer increases in membrane tension. A) Representative walled yeast cells (left column) and protoplasts (right column) at steady state in 1.2 M sorbitol expressing eisosome core protein Pil1-mEGFP (inverted contrast). Note that the cellular concentration of Pil1p-mEGFP is the same in walled cells and protoplasts (panel E). B) Eisosomes labelled with Pil1p-mEGFP (inverted contrast) in wild-type protoplasts at steady state in different sorbitol concentrations. From left to right: 0.25 M, 0.4 M, 0.8 M and 1.2 M sorbitol. C and D) Density of eisosomes at the plasma membrane (C), measured as the ratio between the intensity of Pil1p-mEGFP on the plasma membrane and the surface area of the protoplast and volume (D), at steady state in 0.25 M (N=26), 0.4 M (N=34) and 1.2 M (N=39) sorbitol. Error bars: standard deviations. E) The total amount of Pil1-mEGFP in walled cells (N=32) and protoplasts in 0.4 M sorbitol (N=19) are not significantly different (Mann-Whitney test, P=0.65). Each point represents one measurement, bars are the mean and SEM. F) Micropipette aspiration was used to measure membrane tension. R_c: cell radius; R_p: micropipette radius; l: length of the tongue inside the micropipette. G) Membrane tension of protoplasts at steady state in 0.8 M sorbitol and ~ 5 min after a hypotonic shock ($\Delta C=-0.2$ M) for wild-type (blue bars, N=28 for steady state and N=5 for the shock) and *pil1Δ* protoplasts (red bars, N=42 for steady state and N=7 for the shock). Error bars: standard deviation. p-values: non-significant (ns), $p>0.05$; two stars (**), $p\leq0.01$; three stars (***), $p\leq0.001$. H) and I) Eisosomes of wild-type protoplasts disassemble rapidly after a hypotonic shock. (H) Time course of a representative protoplast expressing Pil1p-mEGFP over 10 minutes after a hypotonic shock ($\Delta C=-0.2$ M) and initially at steady-state in 0.4 M sorbitol (just before time 0 min). (I) Evolution of the surface area covered by eisosomes over time, as a fraction of the surface area covered at time 0 min (normalized to 1). Data are from three independent experiments (N=15) and presented as mean +/- 95% confidence interval. Scale bars in (A), (B), (F) and (H): 5 µm.

Figure 2: Eisosomes protect protoplasts and walled cells from osmotic shocks. A-C) Percentage of wild-type (blue dots) and *pil1Δ* (red triangle) protoplasts that are alive at steady-state in 0.4 M sorbitol, and after a $\Delta C=-0.05$ M (A), $\Delta C=-0.1$ M (B) and $\Delta C=-0.2$ M (C) single hypotonic shock. Representative fields of view used to determine these percentages are shown in Figure 2 – Supplement 1. D) Percentage of wild-type (blue dots) and *pil1Δ* (red triangles) protoplasts that are alive at steady-state in 0.25 M sorbitol, and after a $\Delta C=-0.1$ M hypotonic shock. In these conditions, before the shock eisosomes in wild-type protoplasts are almost completely disassembled (Figure 1B). After the shock, wild-type cells survival is comparable to cells void of eisosomes because they lack Pil1p. E) Timeline of repeated $\Delta C=1.2$ M osmotic shocks for walled cells. Each osmotic shock was performed by exchanging sorbitol concentration from 1.2 M (5 minutes) to 0 M (1 minute). F) Percentage of wild-type (blue dots, N=273) and *pil1Δ* (red triangle, N=197) walled cells that are alive after each osmotic shock. Note the progressive cell death induced by repeated osmotic shocks for *pil1Δ* cells. Combined data are from three independent experiments and plotted as mean +/- standard deviation. G) Representative images of wild-type (upper panel) and *pil1Δ* (lower panel) walled cells before shock and after

the 4th shock. Dead cells are strongly stained by FM4-64 due to membrane damage. Scale bar: 10 µm.

Figure 3: The density of endocytic events rapidly adapts after acute osmotic shocks. A) Temporal evolution of density of endocytic events (average number of endocytic events at a given time in a cell divided by the cell length) in wild-type protoplasts initially at steady state in 0.4 M sorbitol and after an acute hypotonic shock of ΔC=-0.05 M (dark blue, $N_{cell} \geq 102$), ΔC=-0.1M (blue, $N_{cell} \geq 54$) and ΔC=-0.2M (light blue, $N_{cell} \geq 83$). For ΔC=-0.1M and ΔC=-0.2M, the difference in the density of CME events between steady-state and 0 min or 2 min after the shock is statistically significant (one-way ANOVA, $p<10^{-4}$). In all conditions, the difference after 6 min is not significant (one-way ANOVA, $p>0.12$; details in Figure 3 – source data 1). B) Same as (A) but with *pil1Δ* protoplasts and hypotonic shocks of ΔC=-0.025 M (dark red, $N_{cell} \geq 70$), ΔC=-0.05 M (red, $N_{cell} \geq 103$) and ΔC=-0.1 M (light red, $N_{cell} \geq 78$). In all conditions, the difference in the density of CME events between steady-state and any time after the shock is statistically significant (one-way ANOVA, $p<10^{-3}$). For ΔC=-0.025 M and ΔC=-0.05 M, the differences between time points after 6 min are not significant (one-way ANOVA, $p>0.09$; details in Figure 3 – source data 2). (A) and (B) insets: relative volume increase after the hypotonic shocks (the volume at steady state is used as a reference). The numbers of cells used for each condition and each time point are given in Supplementary File 1a. The number of cells measured in the insets are the same as in the main figures. Star (*): the large majority of *pil1Δ* protoplasts were too damaged or dead 4 minutes after the hypotonic shocks at ΔC=-0.1 M (Figure 2B), which prevented us to measure the density of endocytic events and the volume after this time point. C) Density of endocytic events in intact cells at steady state in different osmolarities, $N_{cell} \geq 80$. In *pil1Δ* walled cells, the difference in the density of CME events between all pairs of conditions is statistically significant (one-way ANOVA, $p<10^{-4}$). In wild-type walled cells, the difference is small but statistically significant (details in Figure 3 – source data 3). The numbers of cells used for each condition and each time point are given in Supplementary File 1b. D) Density of endocytic events in wild-type (blue circle) and *pil1Δ* (red triangle) walled cells initially at steady state in 1.2 M sorbitol and after an acute hypotonic shock of ΔC=-1.2M, $N_{cell} \geq 44$. The numbers of cells used for each condition and each time point are given in Supplementary File 1c. For willed-type and *pil1Δ* walled cells, the differences in the density of CME events after 2 min are not statistically significant ($p>0.08$; details Figure 3 – source data 4). (A), (B), (C) and (D): error bars are standard errors of the mean.

Figure 4: Exocytosis rate increases after an acute change in membrane tension in protoplasts but not in walled cells. A) Rationale of measurement of whole cell exocytosis rate through FM4-64 staining. After FM4-64 is flown in the imaging chamber, the dye rapidly binds to the cell surface in less than a minute. After this initial phase, the whole cell fluorescence increases every time new (unlabeled) internal membrane is exposed to the cell surface by exocytosis. Note that endocytic events do not change the total fluorescence measured. B) Measurement of yeast cell exocytosis rate at steady state in 0 M sorbitol. Cells were stained with 20 µM FM4-64 in EMM5S for 20 min before washing with EMM5S. During FM4-64 staining, the fluorescence intensity increases rapidly for 1 min before entering a slow linear phase

over at least 20 min for wild-type cells. The fluorescence intensity at the end of the initial rapid increase phase corresponds to the complete staining of cell surface. It was normalized to 1, so that the subsequent increase in fluorescence intensity corresponds to a percentage of the plasma membrane surface area. After the dye was removed 20 min later, the decrease in fluorescence intensity suggests that the incorporation of FM4-64 didn't interfere with the vesicle trafficking pathway of the cell. The rate of exocytosis (measured as a percentage of the plasma membrane surface area per minute) is the slope of a linear fit of the measured signal over the first 5 min ($k_{0\text{-}5}$), 10 min ($k_{0\text{-}10}$) or 15 min ($k_{0\text{-}15}$). Example images of stained cells at different time points are shown in the middle panel (inverted contrast). (C) - (H) Rates of exocytosis at steady state and after hypotonic shocks. C) and D) The exocytic rate of wild-type walled cells is not changed after a ΔC=-1.2 M acute hypotonic shock (black, before shock, N_{cells}=79; blue, after shock, N_{cells}=68; 3 replicates each). The exocytic rate of *pil1Δ* walled cells does not change significantly in the same conditions (black, before shock, N_{cells}=60; blue, after shock, N_{cells}=96; 3 replicates each). All walled cells were at steady-state in 1.2 M sorbitol before time 0 min. Curves for individual conditions in panels (C) and (D) are plotted in Figures 4 – Supplement 1A and 4 – Supplement 1B, respectively. E) Summary of exocytic rates for wild-type and *pil1Δ* walled cells before and after hypotonic shock. F) and G) The exocytic rate of wild-type and *pil1Δ* protoplasts increases after a ΔC=-0.2 M (black, before shock, N_{cells}=20; light blue, after shock, N_{cells}=37; 4 replicates each) and ΔC=-0.05 M (black, before shock, N_{cells}=44; red, after shock, N_{cells}=60; 4 replicates each) acute hypotonic shocks, respectively. Before time 0 min, all protoplasts were at steady-state in 0.4 M sorbitol. Curves for individual conditions in panels (F) and (G) are plotted in Figures 4 – Supplement 1C and 4 – Supplement 1D, respectively. H) Summary of exocytic rates for wild-type and *pil1Δ* protoplasts before and after hypotonic shock. (C) - (H) Data from at least three independent experiments were pooled together to produce each curve. p-values: non-significant (ns), $p>0.05$; one star (*), $p\leq0.05$; three stars (***), $p\leq0.001$.

Figure 5: Inhibition of exocytosis but not endocytosis decreased the survival rate of protoplasts under acute hypotonic shock. A) *pil1Δ* protoplasts initially at steady state in 0.4 M sorbitol and supplemented with 25 μM Latrunculin A (middle column) or 2 mM Brefeldin A (right column) or nothing (control, left column), were submitted to a ΔC=-0.2 M hypotonic shock (t=0 min). Cells are considered dead if they contain large amounts of intracellular red fluorescence from the FM4-64 dye, which is the consequence of a rupture of the plasma membrane. Scale bar: 10 μm. B) Survival rate for all conditions. Black: control (N=114); blue: 2 mM BFA (N=83); red: 25 μM Latrunculin A (N=70). Data were pooled from two independent experiments and plotted as Kaplan-Meier survival curves. Error bars: standard error of the mean by the Greenwood formula. One star (*), $p\leq0.05$, logrank test.

Figure 6: CME in walled cells is robust over a wide range of conditions. A) Schematic of the plasma membrane deformations and the main components of the actin machinery during CME. Fimbrin (Fim1p, red) crosslinks actin filaments (blue) present at endocytic sites and is used as a proxy to monitor the amount of actin assembled (Figure 6 – Supplement 1). B) Wild-type walled fission yeast cell expressing Fim1p-mEGFP (inverted contrast). Top: cell outlined with a dashed line ;

scale bar: 5 µm. Bottom: montage of a representative CME event. The interval between each frame is 1 s. C) The number of molecules of Fim1p-mEGFP detected, tracked and aligned with temporal super-resolution (Berro and Pollard, 2014c) is highly reproducible between fields of view (one-way ANOVA on the number of molecules at time 0 s, p=0.74). Each curve with a dark color represents the average of several endocytic events from a different field of view of the same sample (N≥64), and the light colors are the 95% confidence intervals. For each average curve, the peak value corresponds to time 0 sec, when vesicle scission happens. D) Number of molecules of Fim1p-mEGFP in wild-type walled cells at steady state in media supplemented with different sorbitol concentrations. There is no statistically significant difference in the number of molecules at time 0 s between the three conditions (one-way ANOVA, p=0.29). N≥388. E) Number of molecules of Fim1p-mEGFP in *pil1Δ* walled cells at steady state in media supplemented with different sorbitol concentrations (N≥342). The difference in the number of molecules at time 0 s between all pairs of conditions is statistically significant (one-way ANOVA, $p<10^{-5}$). F) Timeline of the hypotonic shock experiments and notations. By convention, hypotonic shocks start at time 0 min and are defined by the difference in concentration of sorbitol in the steady state media before the shock (C_{SS}) and after the hypotonic shock (C_{fin}), $\Delta C=C_{fin}-C_{SS}$. Data for a given time point corresponds to endocytic events happening within 1 minute after this time point (e.g. the data at t=0 min correspond to endocytic events happening between 0 and 1 min after the shock). These time intervals are represented by gray bars on the time axis. G) Number of molecules of Fim1p-mEGFP for wild-type walled cells initially at steady state in 1.2 M sorbitol and after an acute osmotic shock of ΔC=-1.2 M. There is no statistically significant difference in the number of molecules at time 0 s between the three conditions (one-way ANOVA, p=0.95). Black: steady state in 1.2 M sorbitol; light to dark blue in top panel: 0 min, 2 min, 4 min, and 6 min after the acute hypotonic shock (N≥103). H) Number of molecules of Fim1p-mEGFP in *pil1Δ* walled cells before and after an acute osmotic shock (ΔC=-1.2 M). The difference in the number of molecules at time 0 s between all pairs of conditions is statistically significant (one-way ANOVA, p<0.03) except between 0 min and 2 min after the shock (one-way ANOVA, p=0.18). Black: steady state in 1.2 M sorbitol before the hypotonic shock (N=583); light to dark red in top panel: 0 min, 2 min and 4 min after the acute hypotonic shock (N≥145). (C), (D), (E), (G) and (H): dark colors: average; light colors: average +/- 95% confidence interval. The number of molecules and speed versus time for each condition are plotted separately in Figure 6 – Supplement 2 (C), Figure 6 – Supplement 3 (D and G), Figure 6 – Supplement 4 (E and H). The numbers of endocytic events used in each curve are given in Supplementary File 1d (C), Supplementary File 1e (D), Supplementary File 1f (E), Supplementary File 1g (G)**,** Supplementary File 1h (H).

Figure 7: The actin endocytic machinery adapts to increases of membrane tension in protoplasts. A) and B) Representative wild-type protoplasts expressing Fim1-mEGFP (inverted contrast) at steady-state in 0.25 M sorbitol (A, left panel) and immediately after (0 min) an acute osmotic shock of ΔC=-0.1 M (B, left panel). Right panels: kymographs of the fluorescence under the yellow lines in the left panels. Black dashed lines: protoplast outline. Scale bars: 5 µm. C) and F) Number of Fim1p-mEGFP molecules in wild-type (C) and *pil1Δ* (F) protoplasts at steady-state in 0.4 M sorbitol (purple), 0 min (brown) and 10 min (orange) after an hypotonic shock of ΔC=-

0.05 M (left panels), ΔC=-0.1 M (middle panels) and ΔC=-0.2 M (right panels), N≥95. Data for each condition are plotted separately in Figures 7 – Supplement 3 (wild type) and 7 – Supplement 4 (*pil1Δ*). The speeds of Fim1p-mEGFP for each condition are shown in Figures 7 – Supplement 5 (wild type) and 7 – Supplement 6 (*pil1Δ*). The numbers of endocytic events used in each curve are given in Supplementary File 1i. Note that the large majority of *pil1Δ* protoplasts were too damaged or dead 2 minutes after hypotonic shocks larger than or equal to ΔC=-0.1 M to allow us to track enough endocytic events and produce a curve (Figures 2B, 2C and 2 – Supplement 1). In panel (C), the difference in the number of molecules at time 0 s at steady state and 0 min after the shock is statistically significant for all shocks (one-way ANOVA, p<0.03) and the difference between steady-state and 10 min after the shock is not statistically significant (one-way ANOVA, p>0.2; details in the data file for figure 7C). In panel (F), the difference at steady state and 0 min after the shock is statistically significant for all shocks (one-way ANOVA, $p<10^{-5}$; details in the data file for figure 5F). D) Temporal adaptation of the peak number of Fim1p-mEGFP in wild-type protoplasts initially at steady state in 0.4 M sorbitol and 0 to 10 min after a ΔC=-0.2 M osmotic shock. The condition for this figure is the same as the condition with the blue star in (C). The difference between steady-state and 0 min or 2 min after shock is statistically significant (one-way ANOVA, $p<10^{-3}$; details in the data file for figure 7D). The difference between steady-state and 4 min, 6 min, 8 min and 10 min after shock is not statistically significant (one-way ANOVA, p>0.2; details in the data file for figure 7D). E) Montage of representative endocytic events (Fim1-mEGFP, inverted contrast) in *pil1Δ* protoplasts (1 frame per second) at steady state in 0.4 M sorbitol (first row) and immediately after (0 min) a hypotonic shocks of ΔC=-0.05 M (second row), ΔC=-0.10 M (third row) and ΔC=-0.20 M (fourth row).G) Temporal adaptation of the peak number of Fim1p-mEGFP in *pil1Δ* protoplasts initially at steady state in 0.4 M sorbitol and 0 to 10 min after a ΔC=-0.05 M shock. The condition in this figure is the same as the condition with the red star in (F). The difference between steady-state and 0 min, 2 min, 4 min, 6 min or 8 min after shock is statistically significant (one-way ANOVA, p<0.01; details in the data file for figure 7F). The difference between steady-state and 10 min after shock is not statistically significant (one-way ANOVA, p>0.3; details in the data file for figure 7F). (D) and (G) error bars are 95% confidence intervals. The numbers of endocytic events at each time point are given in Supplementary File 1j. H) and I) Number of molecules of Fim1p-mEGFP for wild-type (H) and *pil1Δ* (I) protoplasts at steady state in 0.25 M sorbitol (purple dashed) and immediately after (0 min) a hypotonic shock of ΔC=-0.1 M (brown), N≥67. The difference in the number of molecules at time 0 s at steady state and 0 min after the shock is statistically significant for all conditions (one-way ANOVA, $p<10^{-16}$). The speed data for each condition are plotted in Figure 7 – Supplement 7. The numbers of endocytic events used in each curve are given in Supplementary File 1k. The survival rates for the wild-type and *pil1Δ* protoplasts in these conditions are plotted in Figure 2D.

Figure 8: Schematic of the adaptation of fission yeast endocytosis, exocytosis and eisosome after acute hypotonic shock-induced increase in membrane tension. A) In an isotonic solution, endocytosis and exocytosis rates are largely balanced, and proteins including Pil1p are assembled at the plasma membrane to form eisosomes. Actin is recruited to endocytic sites to provide the forces needed to reshape the membrane under normal membrane tension. When present, cell wall

makes fission yeast cell resistant to significant changes in the osmolarity of extracellular solution. B) Acute hypotonic shock results in an increase of membrane tension, which leads to a decrease of endocytosis rate, an increase in exocytosis rate, and a rapid disassembly of eisosomes, within ~2 minutes. The proteins of the actin machinery are recruited in larger amount to endocytic sites to provide larger forces for successful endocytosis under increased membrane tension. Failure of adaptation to the increase in membrane tension leads to membrane rupture and cell death in both protoplasts and walled cells.

Figure Supplements

Figure 2 – Supplement 1: Typical fields of view of protoplasts at steady state in 0.4 M sorbitol and 8 minutes after a ΔC=-0.1 M hypotonic shock. A) Wild-type. B) *pil1Δ*. Cells are considered alive if they do not contain any red fluorescence from the sulforhodamin B dye. Scale bar: 5 µm.

Figure 3 – Supplement 1: Separate plots for each condition shown in Figures 3A and 3B. A) Temporal evolution of density of endocytic events (average number of endocytic events at a given time in a cell divided by the cell length) in wild-type protoplasts initially at steady state in 0.4 M sorbitol and after an acute hypotonic shock of ΔC=-0.05 M (dark blue, $N_{cell}\geq102$), ΔC=-0.1M (blue, $N_{cell}\geq54$) and ΔC=-0.2M (light blue, $N_{cell}\geq83$). B) Same as (A) but with *pil1Δ* protoplasts and hypotonic shocks of ΔC=-0.025 M (dark red, $N_{cell}\geq70$), ΔC=-0.05 M (red, $N_{cell}\geq103$) and ΔC=-0.1 M (light red, $N_{cell}\geq78$). (A) and (B) insets: relative volume increase after the hypotonic shocks (the volume at steady state is used as a reference). The number of cells used for each condition and each time point is given in Supplementary File 1a. The number of cells measured in the insets are the same as in the main figures. (A) and (B): error bars are standard errors of the mean. The number of cells used for each condition and each time point is given in Supplementary File 1b.

Figure 4 – Supplement 1: Separate plots for each condition in Figure 4. Rates of exocytosis at steady state and after hypotonic shocks. A) and B) The exocytic rate of wild-type walled cells is not changed after a ΔC=-1.2 M acute hypotonic shock (black, before shock, $N_{cells}=79$; blue, after shock, $N_{cells}=68$; 3 replicates each). The exocytic rate of *pil1Δ* walled cells does not change significantly in the same conditions (black, before shock, $N_{cells}=60$; blue, after shock, $N_{cells}=96$; 3 replicates each). All walled cells were at steady-state in 1.2 M sorbitol before time 0 min. C) and D) The exocytic rate of wild-type and *pil1Δ* protoplasts increases after a ΔC=-0.2 M (black, before shock, $N_{cells}=20$; light blue, after shock, $N_{cells}=37$; 4 replicates each) and ΔC=-0.05 M (black, before shock, $N_{cells}=44$; red, after shock, $N_{cells}=60$; 4 replicates each) acute hypotonic shocks, respectively. Before time 0 min, all protoplasts were at steady-state in 0.4 M sorbitol. (A)-(D) Dark color: mean; light color: standard error of the mean.

Figure 6 – Supplement 1: Fimbrin is a proxy for actin dynamics during CME in yeast and eisosomes do not participate in CME in wild-type walled cells. A) Colocalization of Fimbrin (mEGFP-Fim1p, green) and End4 (mScarlet-I-End4p, red) during endocytosis. Significant overlapping of signals can be seen in the merged channel. B) Montage of a representative CME event tagged by both mEGFP-Fim1p (top-row) and mScarlet-I-End4p (bottom row). The interval between each frame is 4 s. C) The number of molecules (left panel) and speed (right panel) of Fim1p-mEGFP at CME sites in wild-type (blue, N=1773) and *pil1Δ* (red, N=1884) walled cells at steady state in EMM5S without sorbitol are identical (same data as Figures 6D and 6E). Dark colors: average, light colors: average +/- 95% confidence interval.

Figure 6 – Supplement 2: Speed data (A) and separate plots (B) for the data from each field of view in panel 1C. Each curve with a dark color represents the average of several endocytic events from a different field of view of the same sample (N≥64), and the light colors are the 95% confidence intervals. For each average curve, the peak value corresponds to time 0 sec, when vesicles scission happens. The numbers of endocytic events used in each curve are given in Supplementary File 1d.

Figure 6 – Supplement 3: Representative endocytic events, speeds, and separate plots for each condition in Figures 6D and 6G.
A and B) Speeds corresponding to the data shown in Figures 6D (A) and 6G (B). C) Number of molecules (left panel) and speed (right panel) of Fim1p-mEGFP in wild-type walled cells at steady state in media supplemented with different sorbitol concentrations (N⩾388) (Figure 6D). The numbers of endocytic events used in each curve are given in Supplementary File 1e. D) Number of molecules (left panel) and speed (right panel) of Fim1p-mEGFP for wild-type walled cells initially at steady state in 1.2 M sorbitol and after an acute osmotic shock of ΔC=-1.2 M. Black: steady state in 1.2 M sorbitol; light to dark blue (from top to bottom rows): 0 min, 2 min, 4 min, and 6 min after the acute hypotonic shock (N⩾103) (Figure 6G). The numbers of endocytic events used in each curve are given in Supplementary File 1g. (C) and (D): dark colors: average; light colors: average +/- 95% confidence interval.
E) and F) Left panels: representative wild-type walled cells expressing Fim1p-mEGFP (inverted contrast) at steady state in 1.2 M sorbitol (E) and immediately (0 min) after an acute osmotic shock ΔC=-1.2 M (F). Right panels: kymographs of the fluorescence under the yellow line in the left panels. Black dashed lines: outline of the cell. Scale bars for all panels: 5 µm.

Figure 6 – Supplement 4: Representative endocytic events, speeds, and separate plots for each condition in Figures 6E and 6H.
A and B) Speeds corresponding to the data shown in Figures 6E (A) and 6H (B). C) Number of molecules (left panel) and speed (right panel) of Fim1p-mEGFP in *pil1Δ* walled cells at steady state in media supplemented with different sorbitol concentrations (N⩾342) (Figure 6E). The numbers of endocytic events used in each curve are given in Supplementary File 1e. D) Number of molecules (left panel) and speed (right panel) of Fim1p-mEGFP for wild-type walled cells initially at steady state in 1.2 M sorbitol and after an acute osmotic shock of ΔC=-1.2 M. Black: steady state in 1.2 M sorbitol; light to dark blue (from top to bottom rows): 0 min, 2 min and 4 min after the acute hypotonic shock (N⩾145) (Figure 6H). The numbers of endocytic events used in each curve are given in Supplementary File 1g. (C) and (D): dark colors: average; light colors: average +/- 95% confidence interval.
E) and F) Left panels: representative *pil1Δ* walled cells expressing Fim1p-mEGFP (inverted contrast) at steady state in 1.2 M sorbitol (E) and immediately (0 min) after an acute osmotic shock ΔC=-1.2 M (F). Right panels: kymographs of the fluorescence under the yellow line in the left panels. Black dashed lines: outline of the cell. Scale bars for all panels: 5 µm.

Figure 7 – Supplement 1: CME in protoplasts at steady-state in different sorbitol concentrations. A) Representative walled yeast cells (left column) and protoplasts (right column) at steady state in 1.2 M sorbitol. Top panels: phase contrast; middle panels: cells expressing Fim1-mEGFP (inverted contrast). B) and C) Number of molecules (left panels) and speed (right panels) of Fim1p-mEGFP for wild-type (B) and *pil1Δ* (C) protoplasts at steady state in different sorbitol concentrations. Orange: 0.25 M; purple: 0; green: 0.8 M; black: 1.2 M. Dark colors: average; light colors: average +/- 95% confidence interval (N≥143). Fuchsia dotted curves: wild-type walled cells at steady state in 0 M sorbitol. Data for each condition are plotted separately in Figure 7 – Supplement 2. The numbers of endocytic events used in each curve are given in Supplementary File 1l.

Figure 7 – Supplement 2: Separate plots for each condition in Figure 7 – Supplement 1. A) and B) Number of molecules (left panels) and speed (right panels) of Fim1p-mEGFP for wild-type (A) and *pil1Δ* (B) protoplasts at steady state in different sorbitol concentrations. Orange: 0.25 M; purple: 0; green: 0.8 M; black: 1.2 M. Dark colors: average; light colors: average +/- 95% confidence interval (N≥143). Fuschia dotted curves: walled cells at steady state in 0 M sorbitol (same as Figures 6D and 6E). The numbers of endocytic events used in each curve are given in Supplementary File 1l.

Figure 7 – Supplement 3: Separate plots for each condition shown in Figure 7C. Number of Fim1p-mEGFP molecules in wild-type protoplasts at steady-state in 0.4 M sorbitol (purple), 0 min (brown) and 10 min (orange) after an hypotonic shock of ΔC=-0.05 M (left panels), ΔC=-0.1 M (middle panels) and ΔC=-0.2 M (right panels), N≥95. The speeds of Fim1p-mEGFP for each condition are shown in Figure 7 – Supplement 5. The numbers of endocytic events used in each curve are given in Supplementary File 1i. Dark colors: average, light colors: average +/- 95% confidence interval.

Figure 7 – Supplement 4: Separate plots for each condition shown in Figure 7F. Number of Fim1p-mEGFP molecules in *pil1Δ* protoplasts at steady-state in 0.4 M sorbitol (purple), 0 min (brown) and 10 min (orange) after an hypotonic shock of ΔC=-0.05 M (left panels), ΔC=-0.1 M (middle panels) and ΔC=-0.2 M (right panels), N≥95. The speeds of Fim1p-mEGFP for each condition are shown in Figure 7 – Supplement 6. The numbers of endocytic events used in each curve are given in Supplementary File 1i. Note that the large majority of *pil1Δ* protoplasts were too damaged or dead 2 minutes after hypotonic shocks larger than or equal to ΔC=-0.1 M to allow us to track enough endocytic events and produce a curve (Figures 2B, 2C and 2 – Supplement 1). Dark colors: average, light colors: average +/- 95% confidence interval.

Figure 7 – Supplement 5: Speeds and separate plots for each condition shown in Figure 7C A) Speed of Fim1p-mEGFP in wild-type protoplasts at steady-state in

0.4 M sorbitol (purple), 0 min (brown) and 10 min (orange) after an hypotonic shock of ΔC=-0.05 M (left panels), ΔC=-0.1 M (middle panels) and ΔC=-0.2 M (right panels). B) Separate plots for each condition shown in panel A. (A and B) The same endocytic events as the ones used in Figure 7C have been used to generate these plots. The numbers of endocytic events used in each curve are given in Supplementary File 1i. Dark colors: average, light colors: average +/- 95% confidence interval.

Figure 7 – Supplement 6: Speeds and separate plots for each condition shown in Figure 7F A) Speed of Fim1p-mEGFP in *pil1Δ* protoplasts at steady-state in 0.4 M sorbitol (purple), 0 min (brown) and 10 min (orange) after an hypotonic shock of ΔC=-0.05 M (left panels), ΔC=-0.1 M (middle panels) and ΔC=-0.2 M (right panels). B) Separate plots for each condition shown in panel A. (A and B) The same endocytic events as the ones used in Figure 7F have been used to generate these plots. The numbers of endocytic events used in each curve are given in Supplementary File 1i. Dark colors: average, light colors: average +/- 95% confidence interval.

Figure 7 – Supplement 7: Speed of Fim1p-mEGFP at CME sites for wild-type (A) and *pil1Δ* (B) protoplasts at steady-state in 0.25 M sorbitol (purple) and immediately (0 min) after (brown) a hypotonic shock of ΔC=-0.1 M. The same endocytic events as the ones used in Figures 7H (A) and 7I (B) have been used to generate these plots. The numbers of endocytic events used in each curve are given in Supplementary File 1k. Dark colors: average, light colors: average +/- 95% confidence interval.

Supplementary File

Supplementary file 1: Number of cells used to generate the figures of this paper

a) Figure 3A and Figure 3B
b) Figure 3C
c) Figure 3D
d) Figure 6C and Figure 6 – Supplement 2A
e) Figure 6D
f) Figure 6E
g) Figure 6G
h) Figure 6H
i) Figure 7C and Figure 7F
j) Figure 7D and Figure 7G
k) Figure 7H and Figure 7I
l) Figures 7 – Supplement 1B and Figure 7 – Supplement 1C

Source data files

Figure 1 – source data 1: Data for Figure 1C and 1D

Figure 1 – source data 2: Data for Figure 1E

Figure 1 – source data 3: Data for Figure 1G

Figure 1 – source data 4: Data for Figure 1I

Figure 2 – source data 1: Data for Figure 2A

Figure 2 – source data 2: Data for Figure 2B

Figure 2 – source data 3: Data for Figure 2C

Figure 2 – source data 4: Data for Figure 2D

Figure 2 – source data 5: Data for Figure 2E

Figure 3 – source data 1: Data for Figure 3A

Figure 3 – source data 2: Data for Figure 3B

Figure 3 – source data 3: Data for Figure 3C

Figure 3 – source data 4: Data for Figure 3D

Figure 4 – source data 1: Data for Figure 4B

Figure 4 – source data 2: Data for Figure 4C

Figure 4 – source data 3: Data for Figure 4D

Figure 4 – source data 4: Data for Figure 4E

Figure 4 – source data 5: Data for Figure 4F

Figure 4 – source data 6: Data for Figure 4G

Figure 4 – source data 7: Data for Figure 4H

Figure 5 – source data 1: Data for Figure 5B

Figure 6 – source data 1: Data for Figure 6C and for Figure 6 - Supplement 2

Figure 6 – source data 2: Data for Figure 6D and for Figure 6 - Supplement 3A

Figure 6 – source data 3: Data for Figure 6E and for Figure 6 - Supplement 4A

Figure 6 – source data 4: Data for Figure 6G and for Figure 6 - Supplement 3B

Figure 6 – source data 5: Data for Figure 6H and for Figure 6 - Supplement 4B

Figure 7 – source data 1: Data for Figure 7C

Figure 7 – source data 2: Data for Figure 7D

Figure 7 – source data 3: Data for Figure 7F

Figure 7 – source data 4: Data for Figure 7G

Figure 7 – source data 5: Data for Figure 7H

Figure 7 – source data 6: Data for Figure 7I

Figure 7 – source data 7: Data for Figure 7 - Supplement 1B

Figure 7 – source data 8: Data for Figure 7 - Supplement 1C

Figure 7 – source data 9: Data for Figure 7 - Supplement 5

Figure 7 – source data 10: Data for Figure 7 - Supplement 6

Figure 7 – source data 11: Data for Figure 7 - Supplement 7

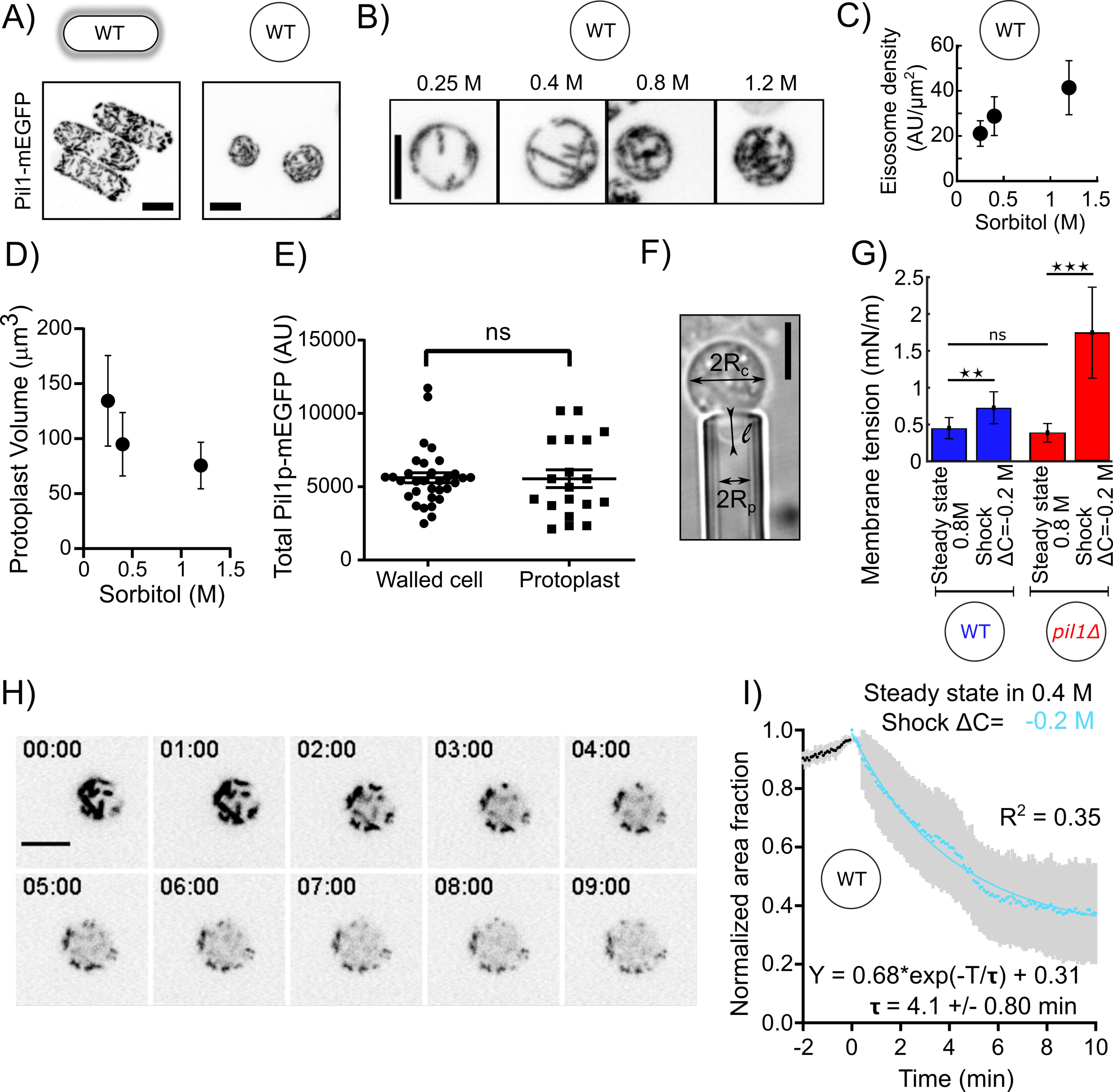

A)
WT
WT
Pil1-mEGFP
B)
WT
0.25 M
0.4 M
0.8 M
1.2 M
C)
WT
Eisosome density (AU/µm²)
Sorbitol (M)
D)
Protoplast Volume (µm³)
Sorbitol (M)
E)
ns
Total Pil1p-mEGFP (AU)
Walled cell
Protoplast
F)
2Rc
ℓ
2Rp
G)
Membrane tension (mN/m)
ns
Steady state 0.8M
Shock ΔC=-0.2 M
Steady state 0.8 M
Shock ΔC=-0.2 M
WT
pil1Δ
H)
00:00
01:00
02:00
03:00
04:00
05:00
06:00
07:00
08:00
09:00
I)
Steady state in 0.4 M
Shock ΔC= -0.2 M
R² = 0.35
WT
Normalized area fraction
Y = 0.68*exp(-T/τ) + 0.31
τ = 4.1 +/- 0.80 min
Time (min)

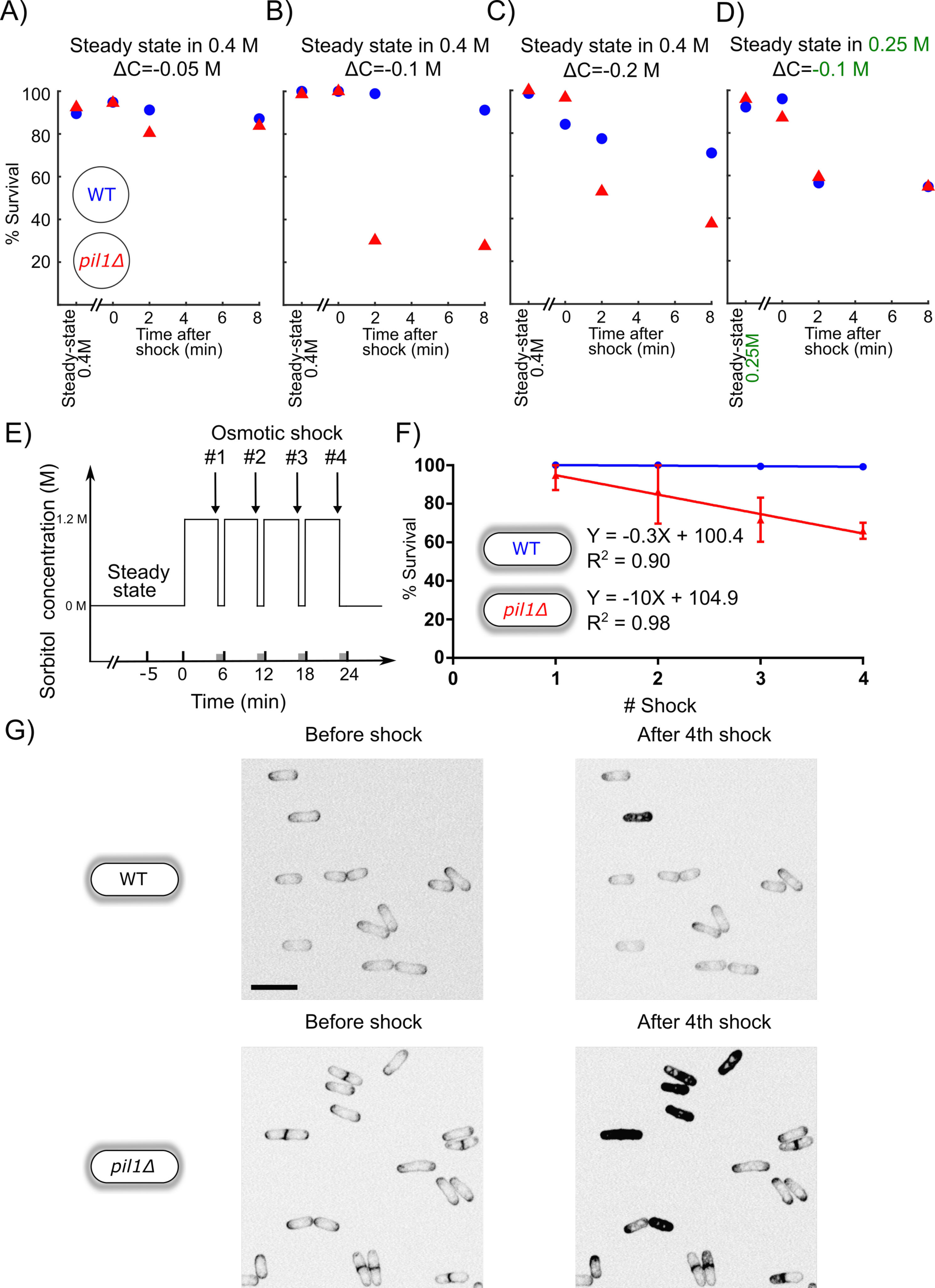

A)
Steady state in 0.4 M
ΔC=-0.05 M
B)
Steady state in 0.4 M
ΔC=-0.1 M
C)
Steady state in 0.4 M
ΔC=-0.2 M
D)
Steady state in 0.25 M
ΔC=-0.1 M
% Survival
100
80
60
40
20
WT
pil1Δ
Steady-state 0.4M
Steady-state 0.25M
0
2
4
6
8
Time after shock (min)
E)
Osmotic shock
#1 #2 #3 #4
Sorbitol concentration (M)
1.2 M
0 M
Steady state
-5 0 6 12 18 24
Time (min)
F)
% Survival
# Shock
WT
Y = -0.3X + 100.4
R2 = 0.90
pil1Δ
Y = -10X + 104.9
R2 = 0.98
0 1 2 3 4
G)
Before shock
After 4th shock
WT
pil1Δ

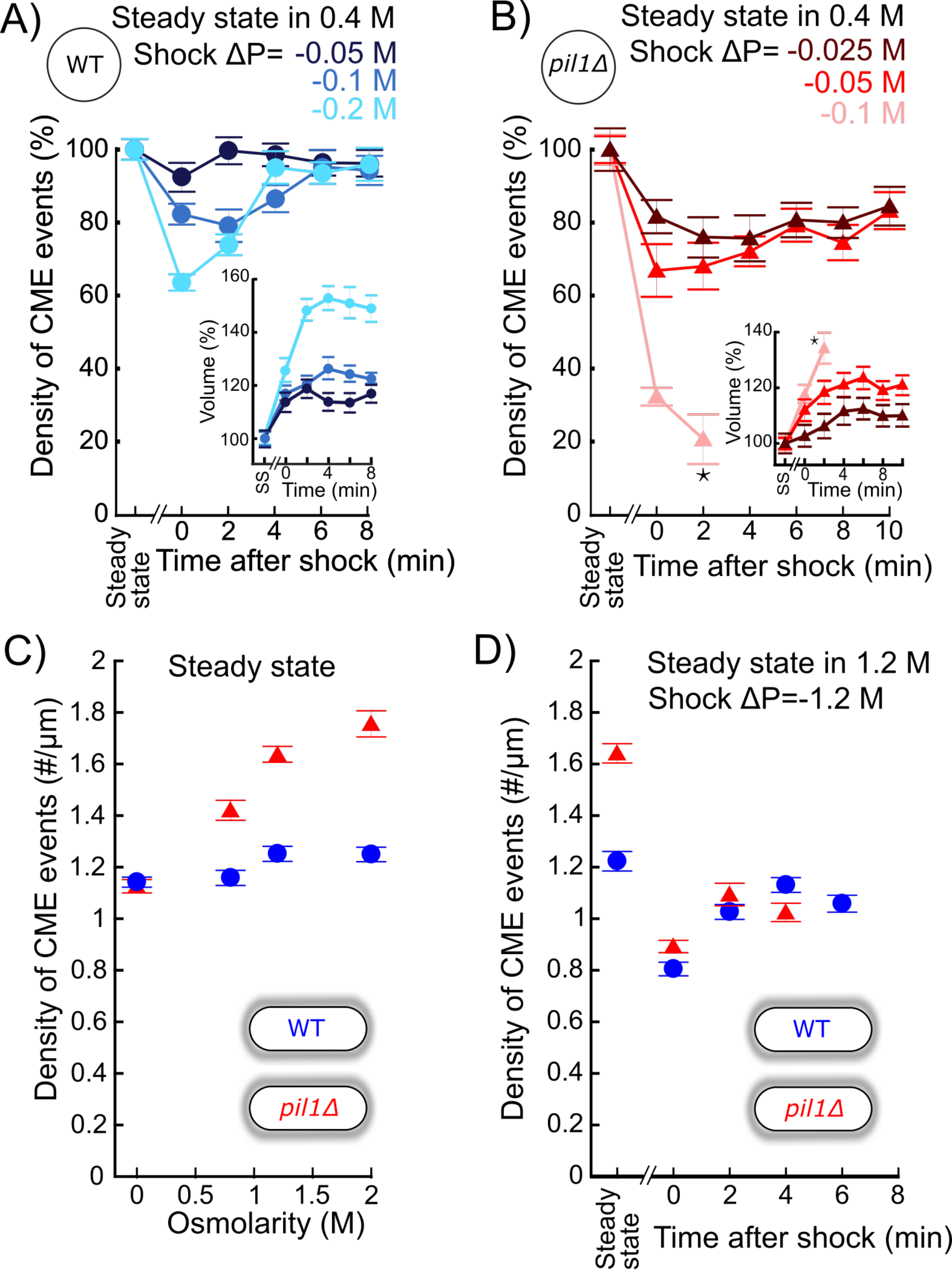

A)
WT
Steady state in 0.4 M
Shock ΔP= -0.05 M
-0.1 M
-0.2 M
Density of CME events (%)
Volume (%)
Time (min)
SS
Steady state
Time after shock (min)
B)
pil1Δ
Steady state in 0.4 M
Shock ΔP= -0.025 M
-0.05 M
-0.1 M
C)
Steady state
Density of CME events (#/μm)
Osmolarity (M)
WT
pil1Δ
D)
Steady state in 1.2 M
Shock ΔP=-1.2 M

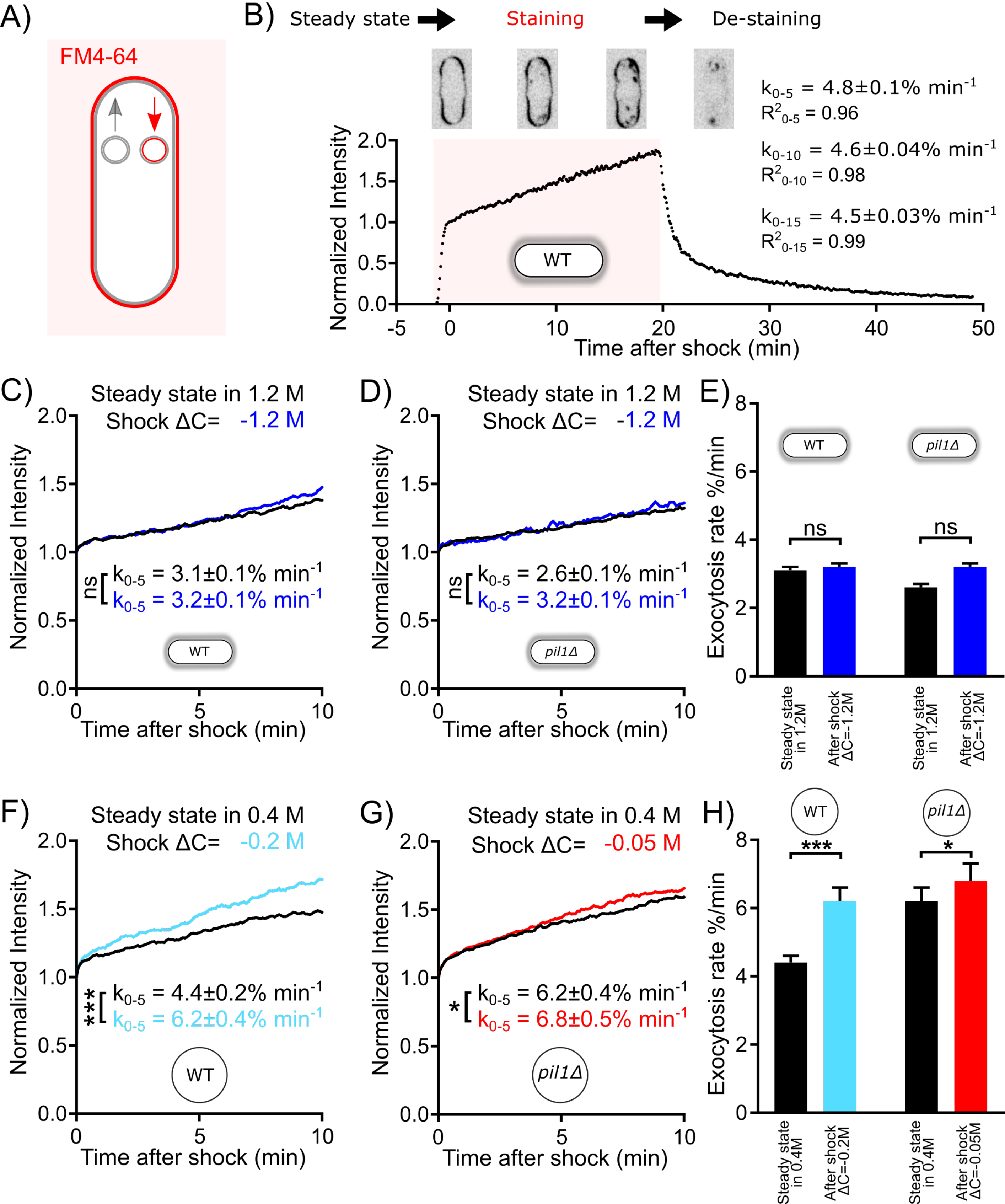

A)
FM4-64
B)
Steady state
Staining
De-staining
k_{0-5} = 4.8±0.1% min^{-1}
R^2_{0-5} = 0.96
k_{0-10} = 4.6±0.04% min^{-1}
R^2_{0-10} = 0.98
k_{0-15} = 4.5±0.03% min^{-1}
R^2_{0-15} = 0.99
WT
Normalized Intensity
Time after shock (min)
C)
Steady state in 1.2 M
Shock ΔC= -1.2 M
ns
k_{0-5} = 3.1±0.1% min^{-1}
k_{0-5} = 3.2±0.1% min^{-1}
WT
Normalized Intensity
Time after shock (min)
D)
Steady state in 1.2 M
Shock ΔC= -1.2 M
ns
k_{0-5} = 2.6±0.1% min^{-1}
k_{0-5} = 3.2±0.1% min^{-1}
pil1Δ
Normalized Intensity
Time after shock (min)
E)
Exocytosis rate %/min
WT
pil1Δ
ns
ns
Steady state in 1.2M
After shock ΔC=-1.2M
Steady state in 1.2M
After shock ΔC=-1.2M
F)
Steady state in 0.4 M
Shock ΔC= -0.2 M
***
k_{0-5} = 4.4±0.2% min^{-1}
k_{0-5} = 6.2±0.4% min^{-1}
WT
Normalized Intensity
Time after shock (min)
G)
Steady state in 0.4 M
Shock ΔC= -0.05 M
*
k_{0-5} = 6.2±0.4% min^{-1}
k_{0-5} = 6.8±0.5% min^{-1}
pil1Δ
Normalized Intensity
Time after shock (min)
H)
WT
pil1Δ
***
*
Exocytosis rate %/min
Steady state in 0.4M
After shock ΔC=-0.2M
Steady state in 0.4M
After shock ΔC=-0.05M

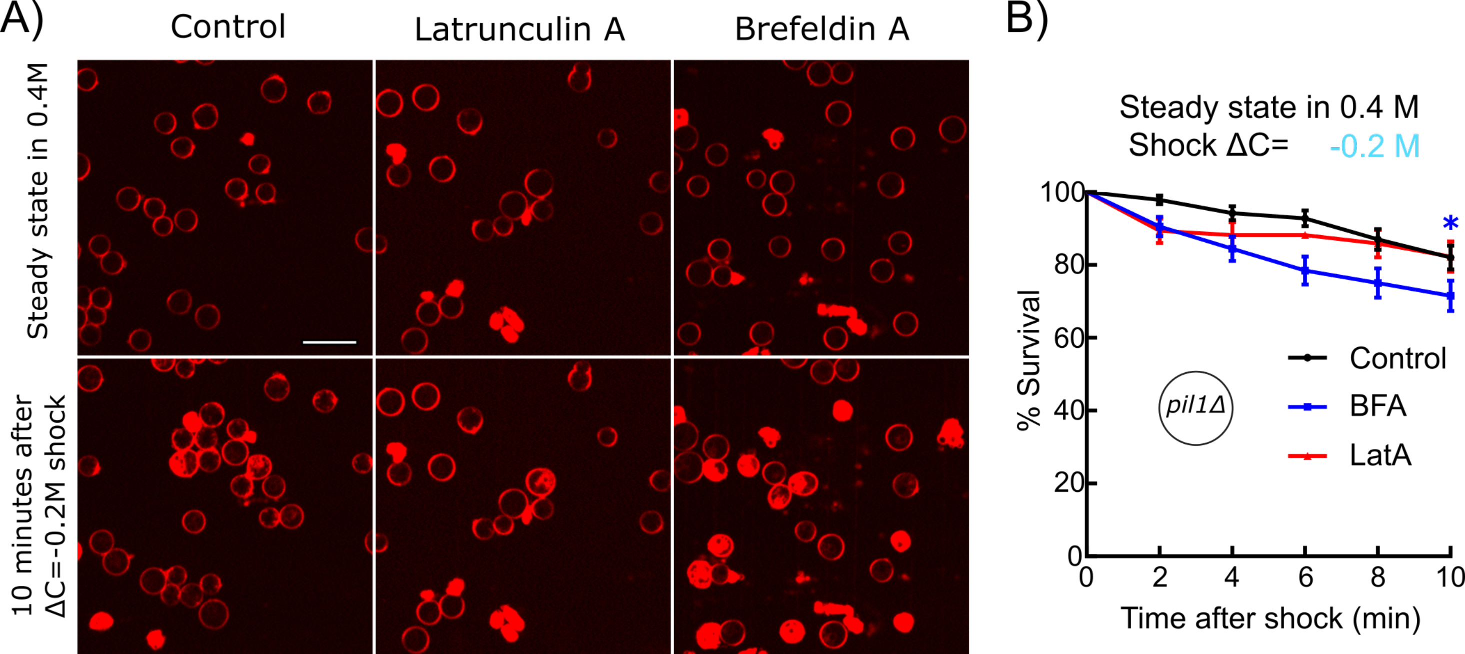
A)
Control
Latrunculin A
Brefeldin A
Steady state in 0.4M
10 minutes after ΔC=-0.2M shock
B)
Steady state in 0.4 M
Shock ΔC= -0.2 M
% Survival
Time after shock (min)
pil1Δ
Control
BFA
LatA
*
0
20
40
60
80
100
0
2
4
6
8
10

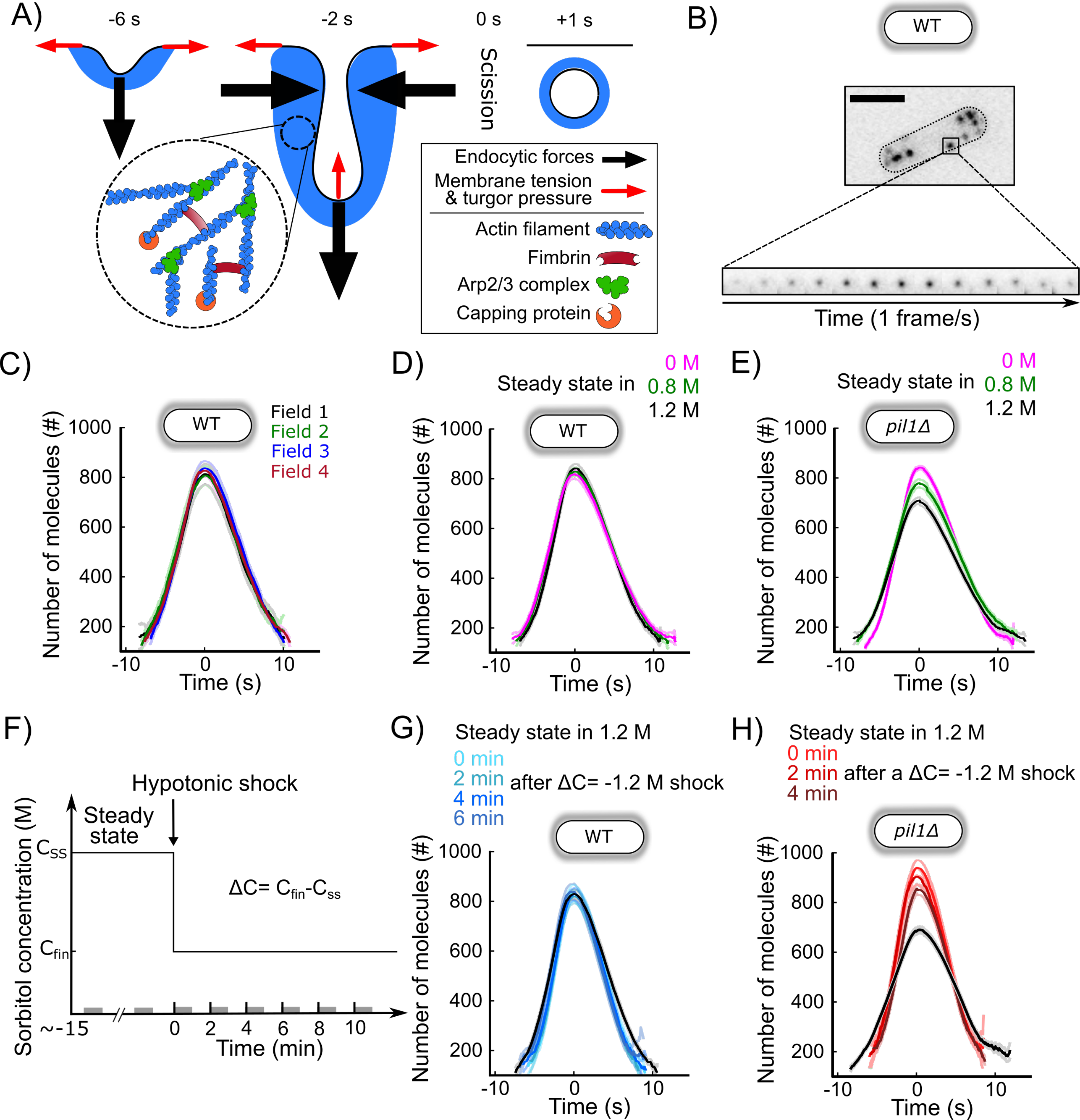
A)
-6 s
-2 s
0 s
+1 s
Scission
Endocytic forces
Membrane tension & turgor pressure
Actin filament
Fimbrin
Arp2/3 complex
Capping protein
B)
WT
Time (1 frame/s)
C)
WT
Field 1
Field 2
Field 3
Field 4
Number of molecules (#)
Time (s)
D)
Steady state in
0 M
0.8 M
1.2 M
WT
Number of molecules (#)
Time (s)
E)
Steady state in
0 M
0.8 M
1.2 M
pil1Δ
Number of molecules (#)
Time (s)
F)
Hypotonic shock
Steady state
Sorbitol concentration (M)
C_{ss}
C_{fin}
$\Delta C = C_{fin} - C_{ss}$
~-15
0 2 4 6 8 10
Time (min)
G)
Steady state in 1.2 M
0 min
2 min after ΔC= -1.2 M shock
4 min
6 min
WT
Number of molecules (#)
Time (s)
H)
Steady state in 1.2 M
0 min
2 min after a ΔC= -1.2 M shock
4 min
pil1Δ
Number of molecules (#)
Time (s)

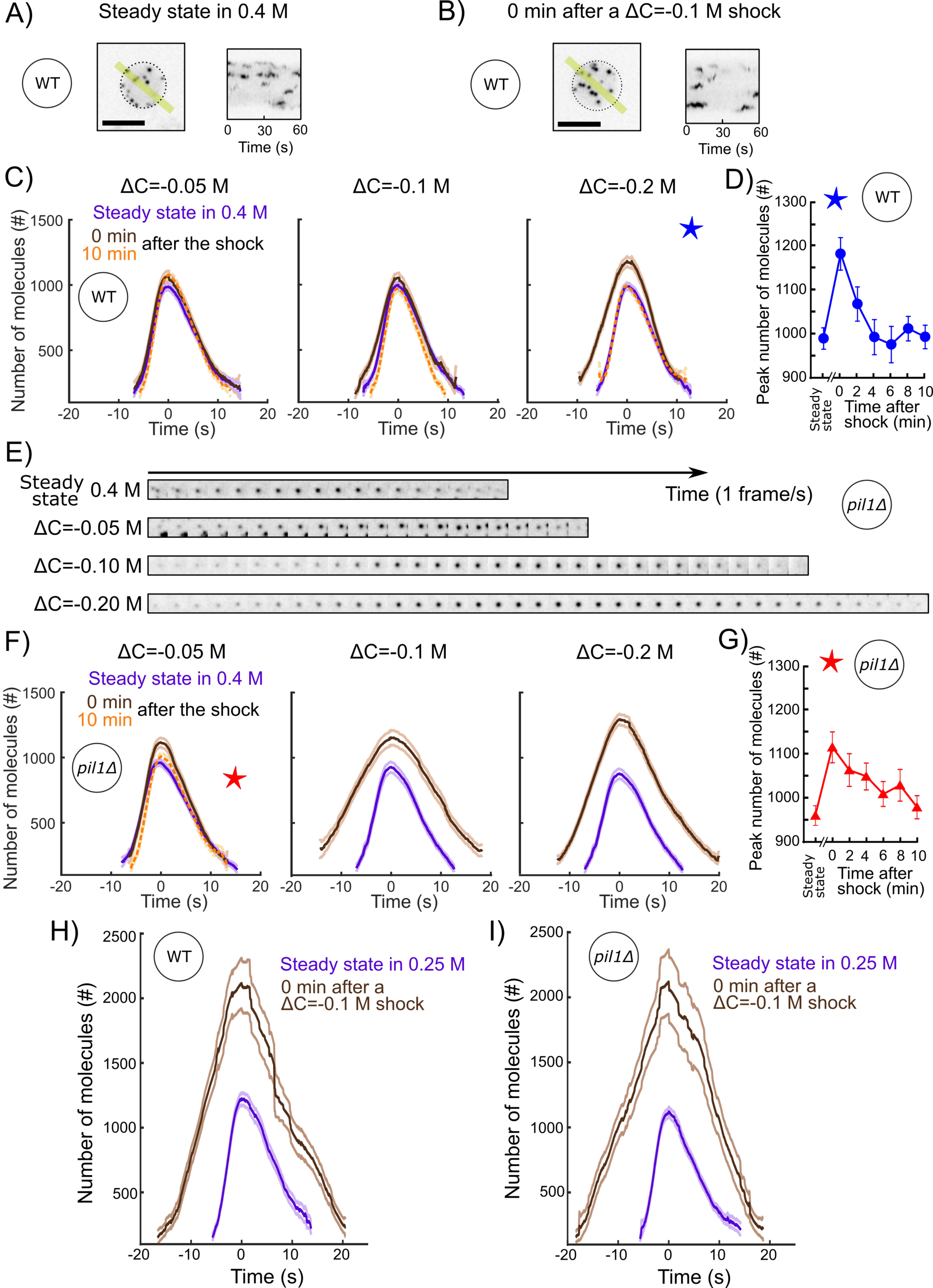

A)
Steady state in 0.4 M
WT
0
30
60
Time (s)
B)
0 min after a ΔC=-0.1 M shock
WT
0
30
60
Time (s)
C)
ΔC=-0.05 M
ΔC=-0.1 M
ΔC=-0.2 M
Steady state in 0.4 M
0 min
10 min
after the shock
WT
Number of molecules (#)
1500
1000
500
-20
-10
0
10
20
Time (s)
D)
WT
Peak number of molecules (#)
1300
1200
1100
1000
900
Steady state
0
2
4
6
8
10
Time after shock (min)
E)
Steady state
0.4 M
ΔC=-0.05 M
ΔC=-0.10 M
ΔC=-0.20 M
Time (1 frame/s)
pil1Δ
F)
ΔC=-0.05 M
ΔC=-0.1 M
ΔC=-0.2 M
Steady state in 0.4 M
0 min
10 min
after the shock
pil1Δ
Number of molecules (#)
1500
1000
500
-20
-10
0
10
20
Time (s)
G)
pil1Δ
Peak number of molecules (#)
1300
1200
1100
1000
900
Steady state
0
2
4
6
8
10
Time after shock (min)
H)
WT
Steady state in 0.25 M
0 min after a
ΔC=-0.1 M shock
Number of molecules (#)
2500
2000
1500
1000
500
-20
-10
0
10
20
Time (s)
I)
pil1Δ
Steady state in 0.25 M
0 min after a
ΔC=-0.1 M shock
Number of molecules (#)
2500
2000
1500
1000
500
-20
-10
0
10
20
Time (s)

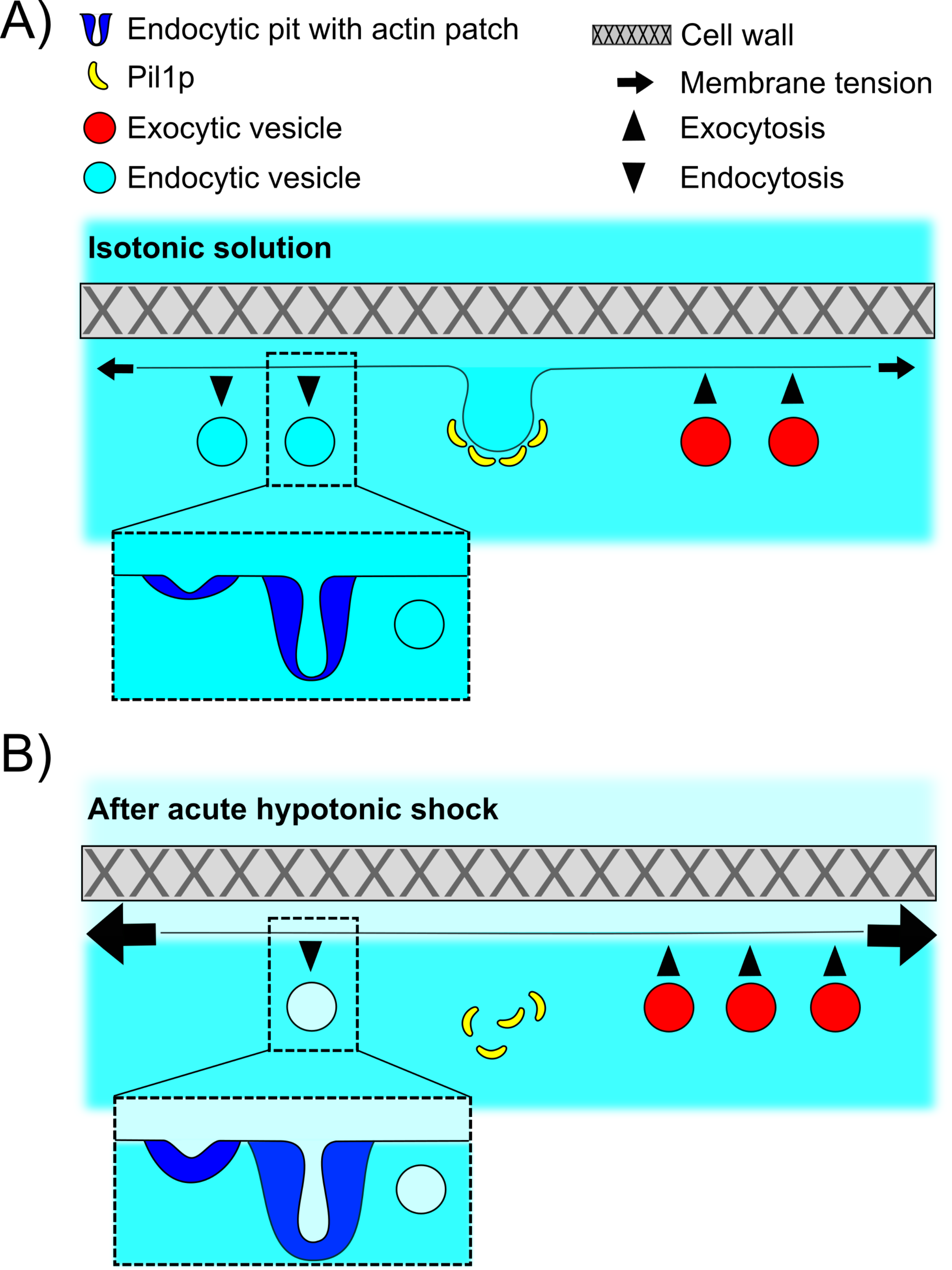
A)
Endocytic pit with actin patch
Pil1p
Exocytic vesicle
Endocytic vesicle
Cell wall
Membrane tension
Exocytosis
Endocytosis
Isotonic solution
B)
After acute hypotonic shock

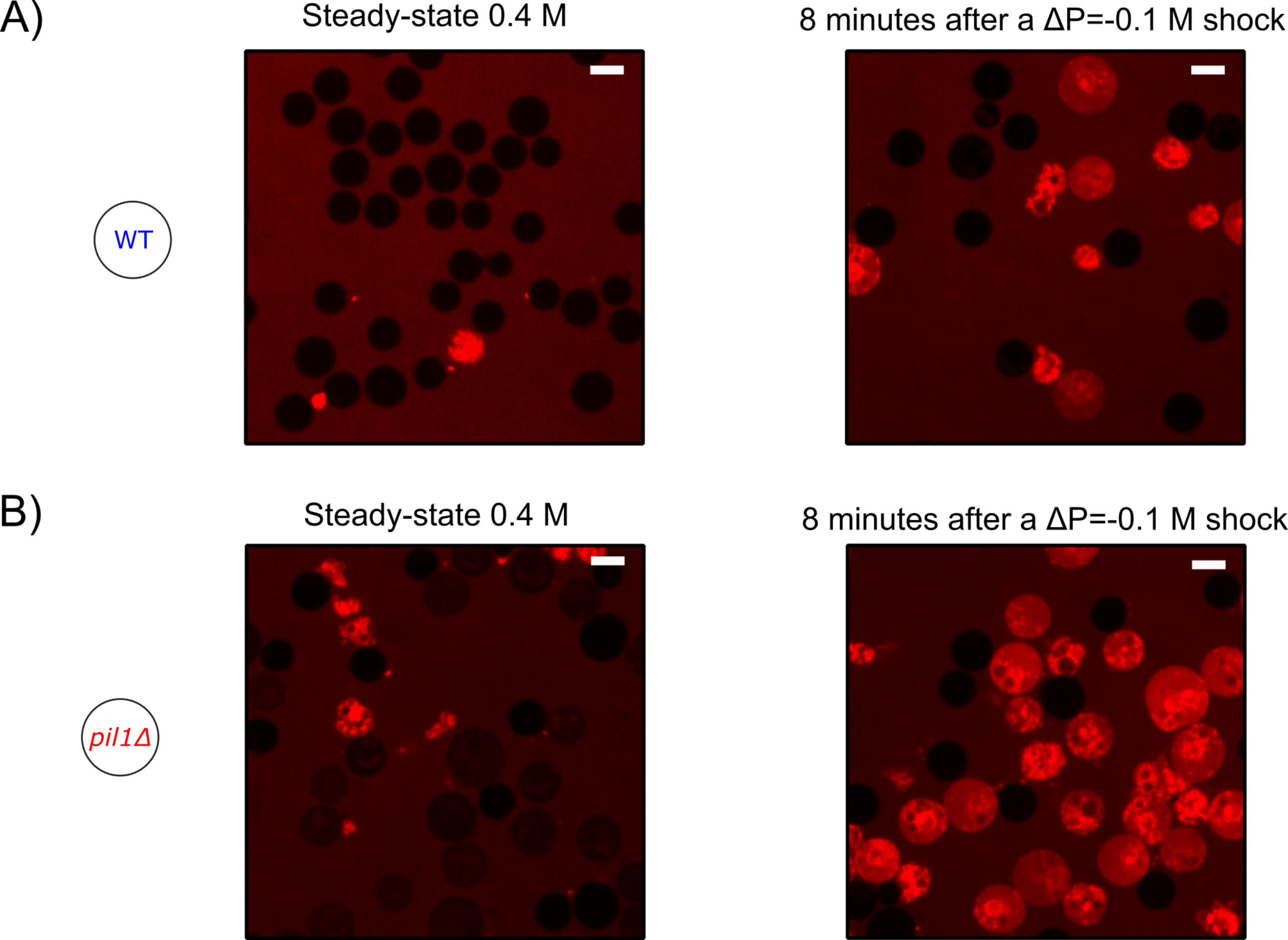
A)
Steady-state 0.4 M
8 minutes after a ΔP=-0.1 M shock
WT
B)
Steady-state 0.4 M
8 minutes after a ΔP=-0.1 M shock
pil1Δ

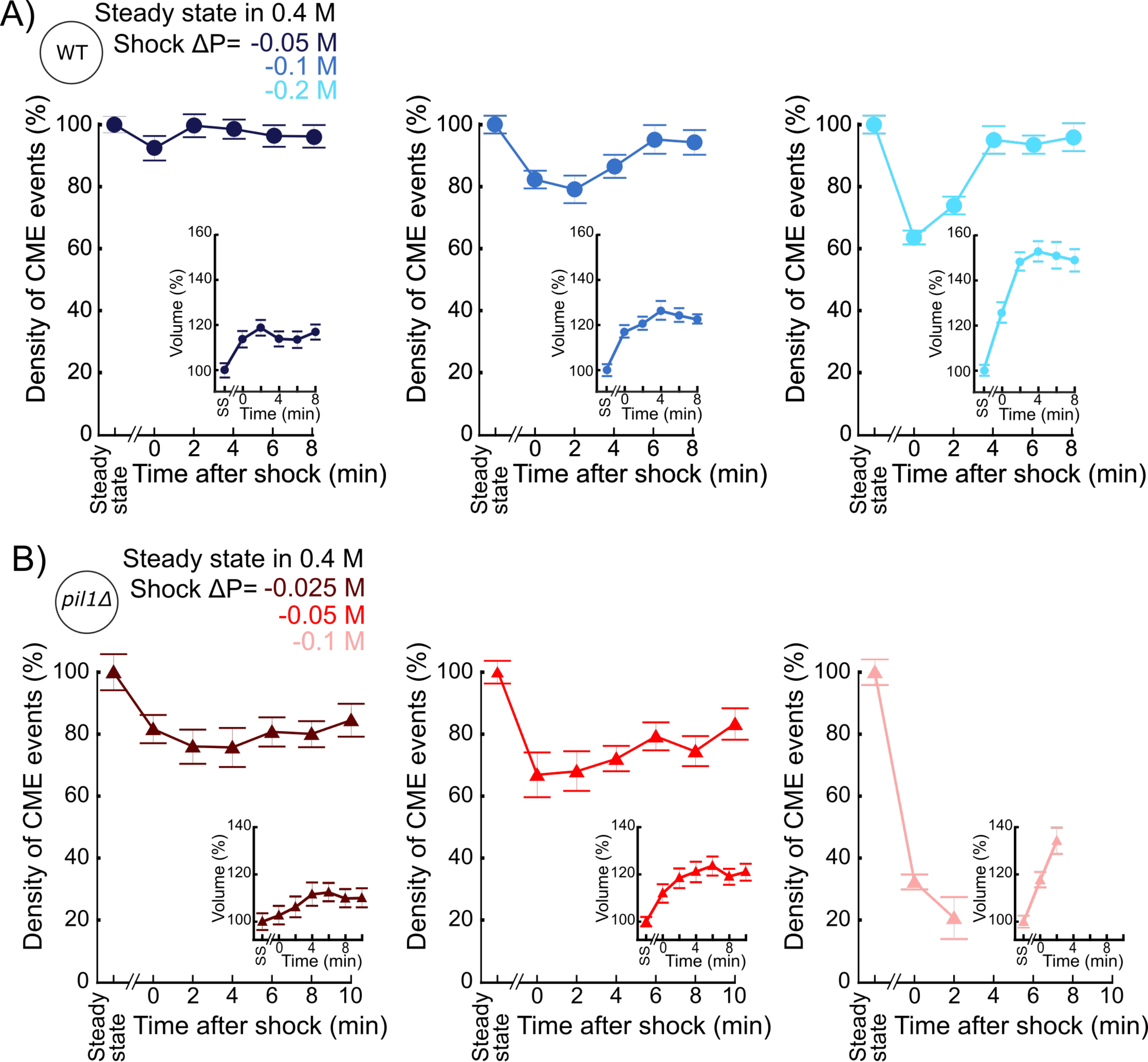

A)
WT
Steady state in 0.4 M
Shock ΔP= -0.05 M
-0.1 M
-0.2 M
Density of CME events (%)
Volume (%)
Time (min)
SS
Steady state
Time after shock (min)
B)
pil1Δ
Steady state in 0.4 M
Shock ΔP= -0.025 M
-0.05 M
-0.1 M
Density of CME events (%)
Volume (%)
Time (min)
SS
Steady state
Time after shock (min)

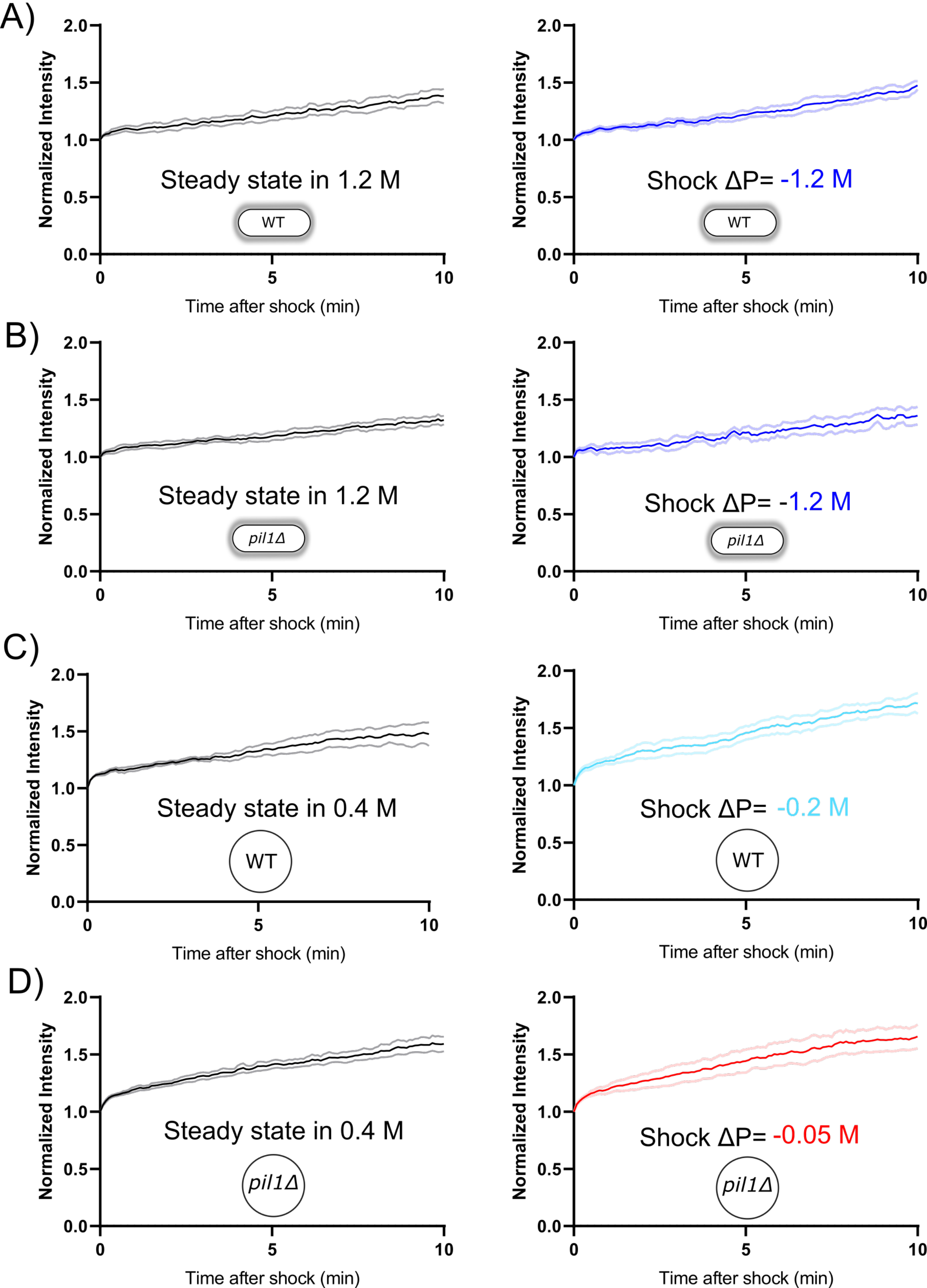
A)
Steady state in 1.2 M
WT
Shock ΔP= -1.2 M
WT
B)
Steady state in 1.2 M
pil1Δ
Shock ΔP= -1.2 M
pil1Δ
C)
Steady state in 0.4 M
WT
Shock ΔP= -0.2 M
WT
D)
Steady state in 0.4 M
pil1Δ
Shock ΔP= -0.05 M
pil1Δ
Normalized Intensity
Time after shock (min)

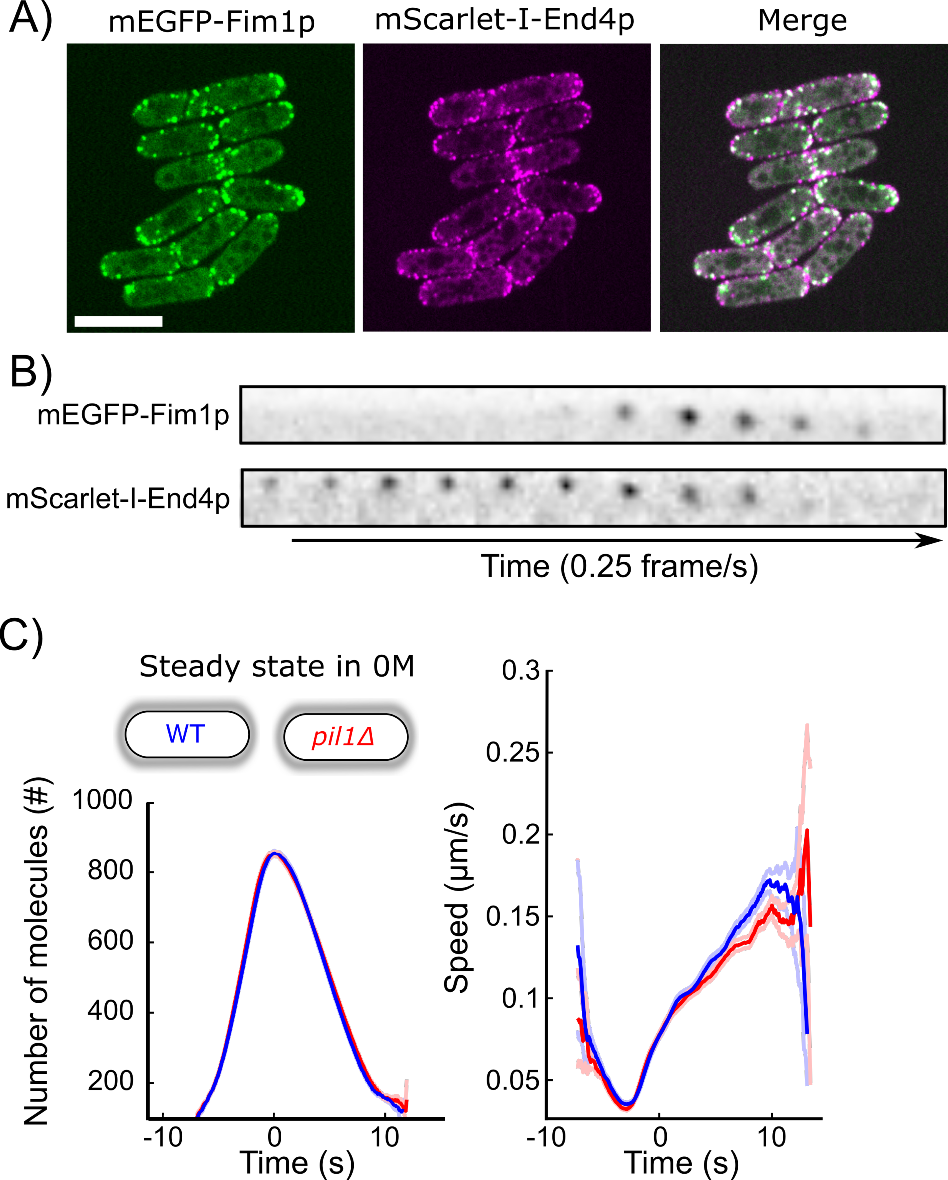

A)
mEGFP-Fim1p
mScarlet-I-End4p
Merge
B)
mEGFP-Fim1p
mScarlet-I-End4p
Time (0.25 frame/s)
C)
Steady state in 0M
WT
pil1Δ
Number of molecules (#)
1000
800
600
400
200
-10
0
10
Time (s)
Speed (µm/s)
0.3
0.25
0.2
0.15
0.1
0.05
-10
0
10
Time (s)

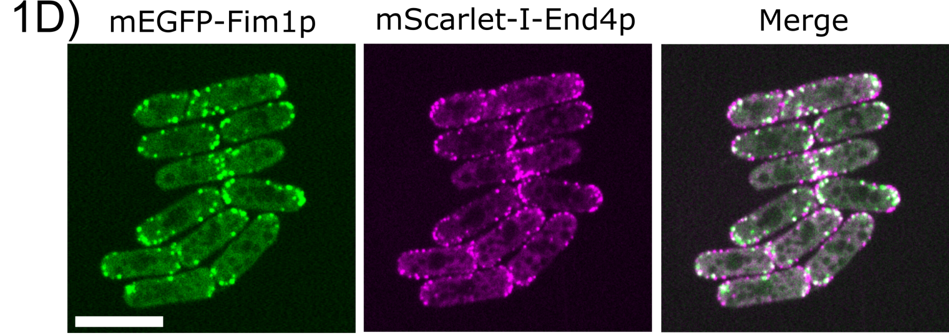

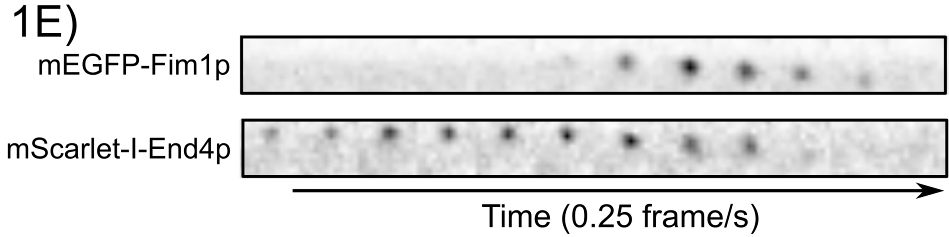

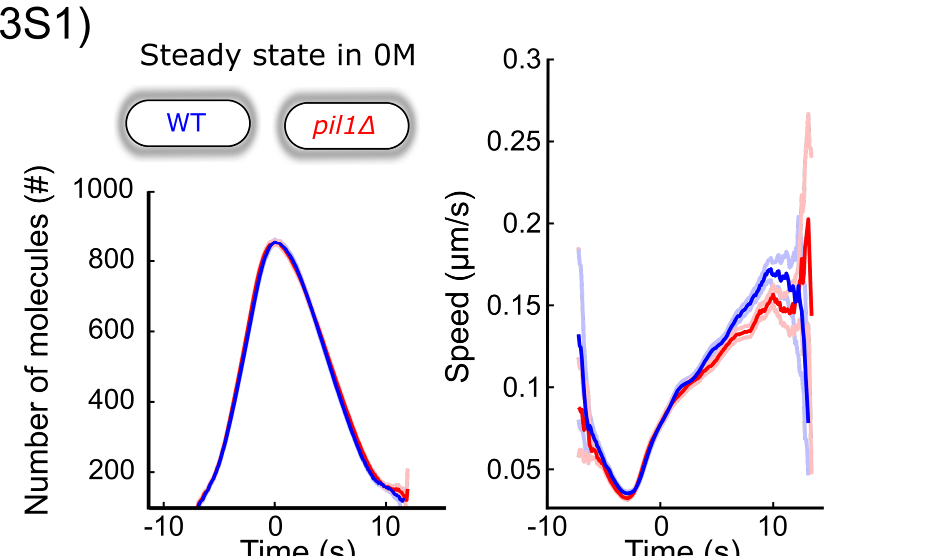

TODO:
update panel numbers

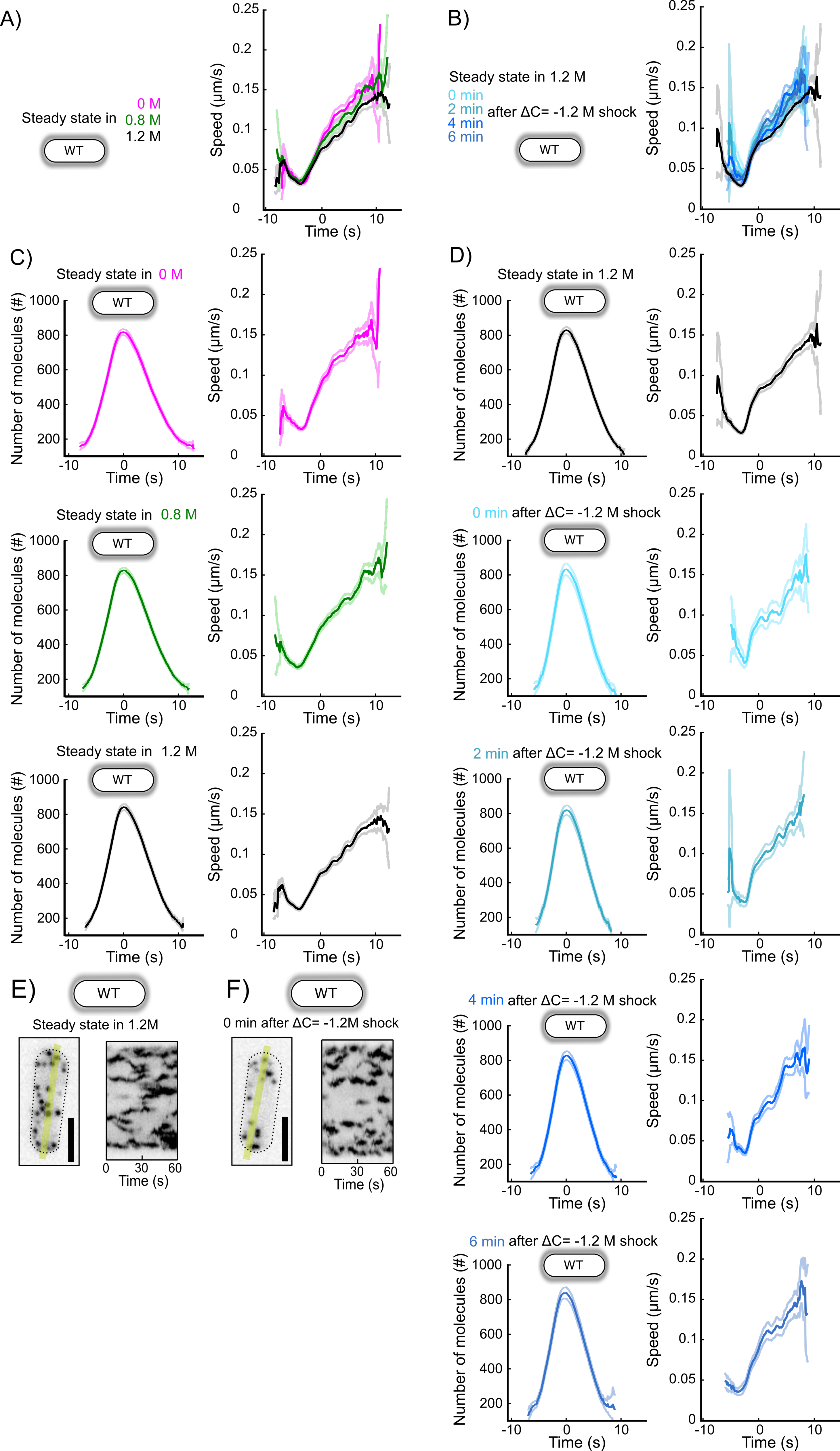

A)
Steady state in
0 M
0.8 M
1.2 M
WT
Speed (µm/s)
Time (s)
B)
Steady state in 1.2 M
0 min
2 min
4 min
6 min
after ΔC= -1.2 M shock
WT
Speed (µm/s)
Time (s)
C)
Steady state in 0 M
Steady state in 0.8 M
Steady state in 1.2 M
Number of molecules (#)
Speed (µm/s)
Time (s)
D)
Steady state in 1.2 M
0 min after ΔC= -1.2 M shock
2 min after ΔC= -1.2 M shock
4 min after ΔC= -1.2 M shock
6 min after ΔC= -1.2 M shock
Number of molecules (#)
Speed (µm/s)
Time (s)
E)
WT
Steady state in 1.2M
Time (s)
F)
WT
0 min after ΔC= -1.2M shock
Time (s)

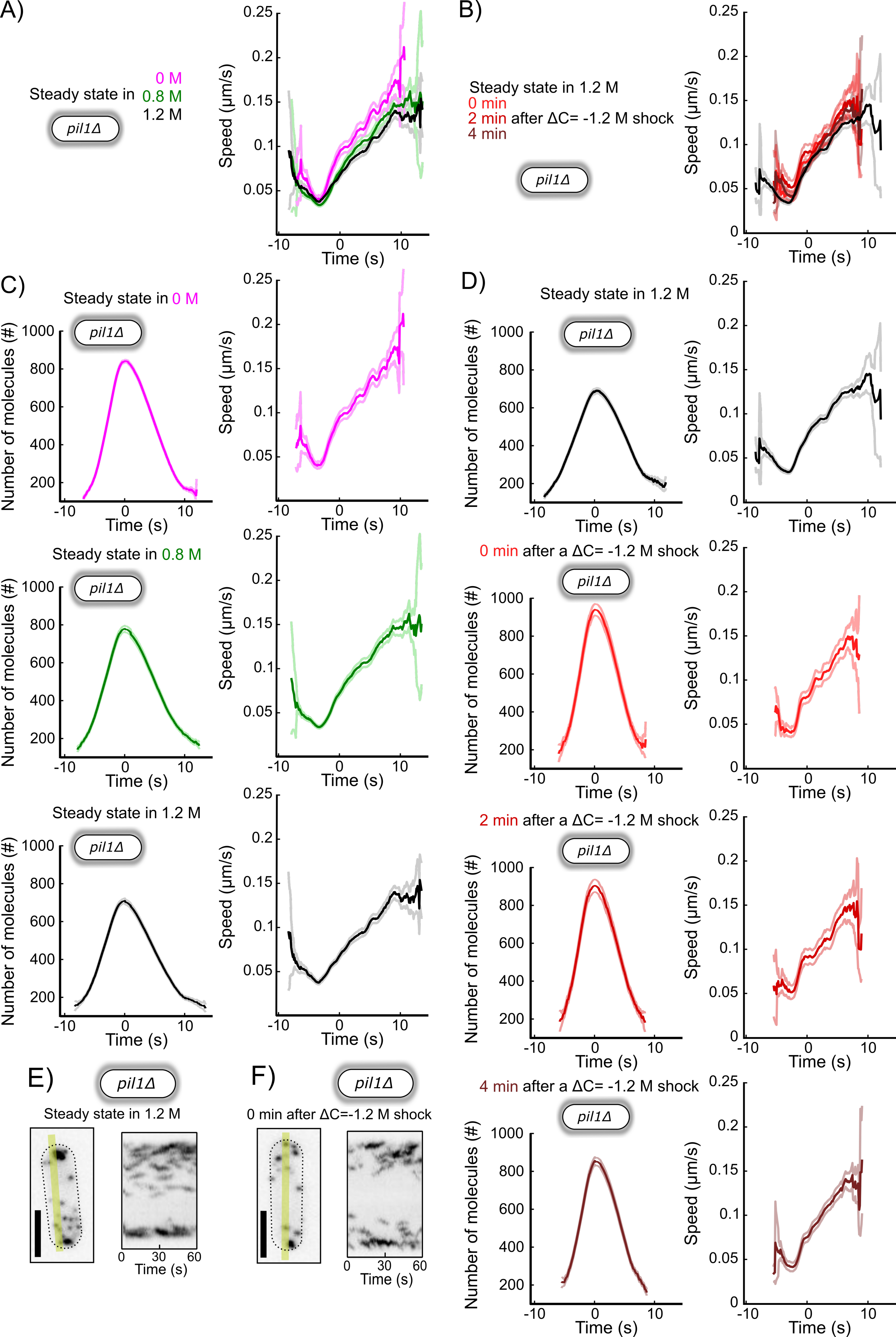
A)
Steady state in
0 M
0.8 M
1.2 M
pil1Δ
Speed (μm/s)
Time (s)
B)
Steady state in 1.2 M
0 min
2 min after ΔC= -1.2 M shock
4 min
pil1Δ
Speed (μm/s)
Time (s)
C)
Steady state in 0 M
pil1Δ
Number of molecules (#)
Time (s)
Speed (μm/s)
Time (s)
Steady state in 0.8 M
pil1Δ
Number of molecules (#)
Time (s)
Speed (μm/s)
Time (s)
Steady state in 1.2 M
pil1Δ
Number of molecules (#)
Time (s)
Speed (μm/s)
Time (s)
D)
Steady state in 1.2 M
pil1Δ
Number of molecules (#)
Time (s)
Speed (μm/s)
Time (s)
0 min after a ΔC= -1.2 M shock
pil1Δ
Number of molecules (#)
Time (s)
Speed (μm/s)
Time (s)
2 min after a ΔC= -1.2 M shock
pil1Δ
Number of molecules (#)
Time (s)
Speed (μm/s)
Time (s)
4 min after a ΔC= -1.2 M shock
pil1Δ
Number of molecules (#)
Time (s)
Speed (μm/s)
Time (s)
E)
pil1Δ
Steady state in 1.2 M
0
30
60
Time (s)
F)
pil1Δ
0 min after ΔC=-1.2 M shock
0
30
60
Time (s)

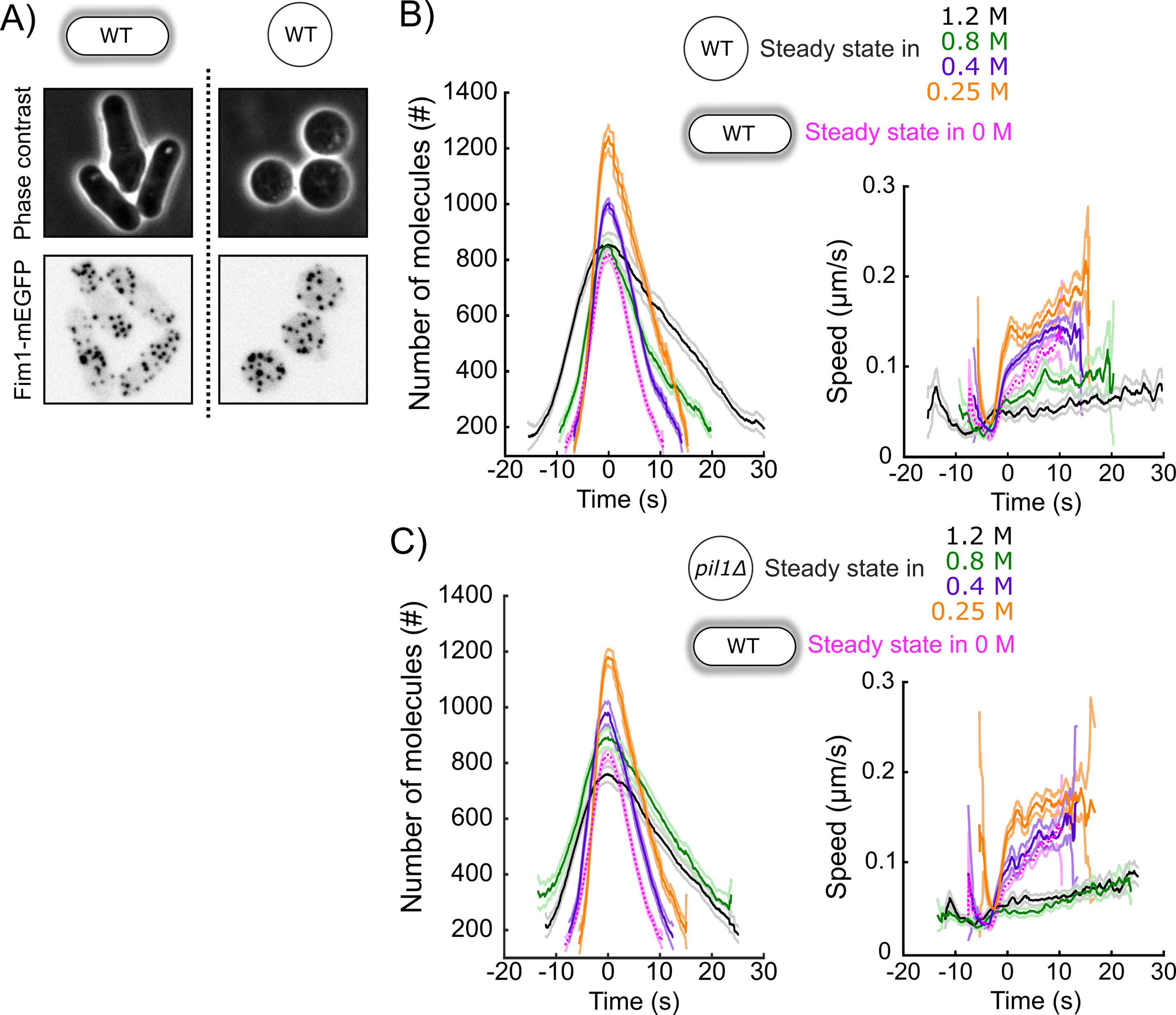

A)
WT
WT
Phase contrast
Fim1-mEGFP
B)
WT Steady state in
1.2 M
0.8 M
0.4 M
0.25 M
WT Steady state in 0 M
Number of molecules (#)
Time (s)
Speed (µm/s)
Time (s)
C)
pil1Δ Steady state in
1.2 M
0.8 M
0.4 M
0.25 M
WT Steady state in 0 M
Number of molecules (#)
Time (s)
Speed (µm/s)
Time (s)

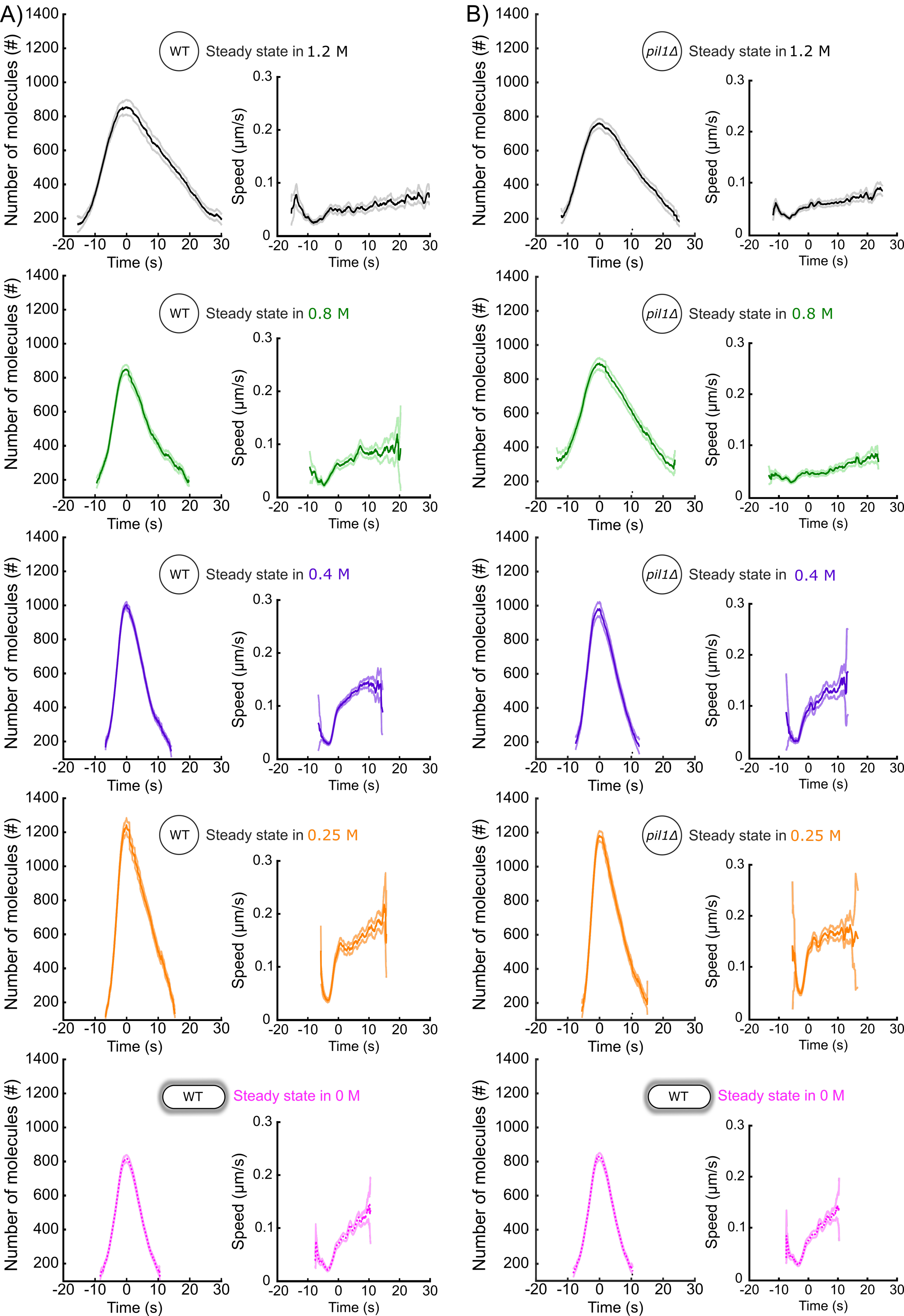
A)
B)
WT Steady state in 1.2 M
WT Steady state in 0.8 M
WT Steady state in 0.4 M
WT Steady state in 0.25 M
WT Steady state in 0 M
pil1Δ Steady state in 1.2 M
pil1Δ Steady state in 0.8 M
pil1Δ Steady state in 0.4 M
pil1Δ Steady state in 0.25 M
Number of molecules (#)
Speed (µm/s)
Time (s)

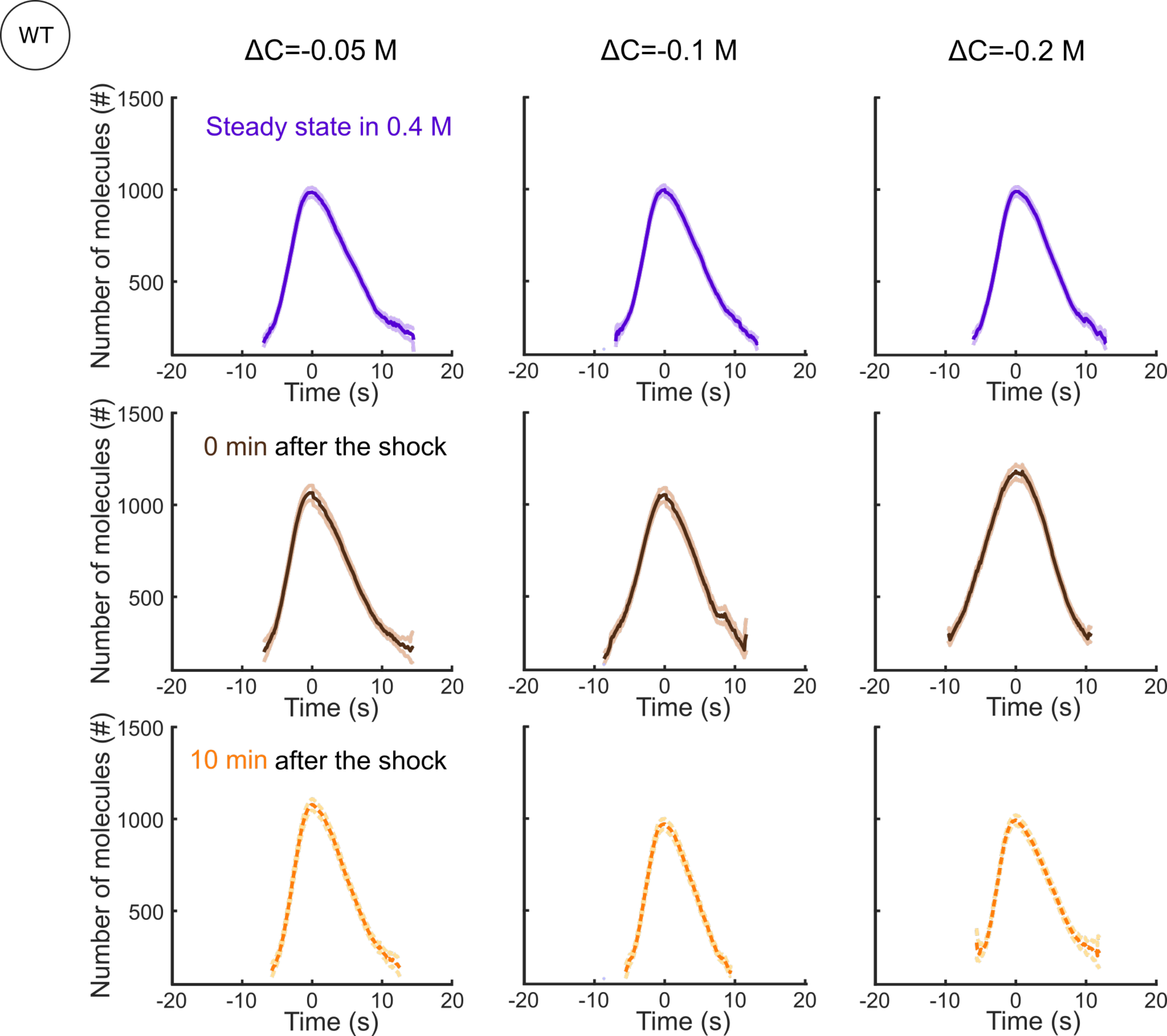
WT
ΔC=-0.05 M
ΔC=-0.1 M
ΔC=-0.2 M
Steady state in 0.4 M
0 min after the shock
10 min after the shock
Number of molecules (#)
Time (s)
1500
1000
500
-20
-10
0
10
20

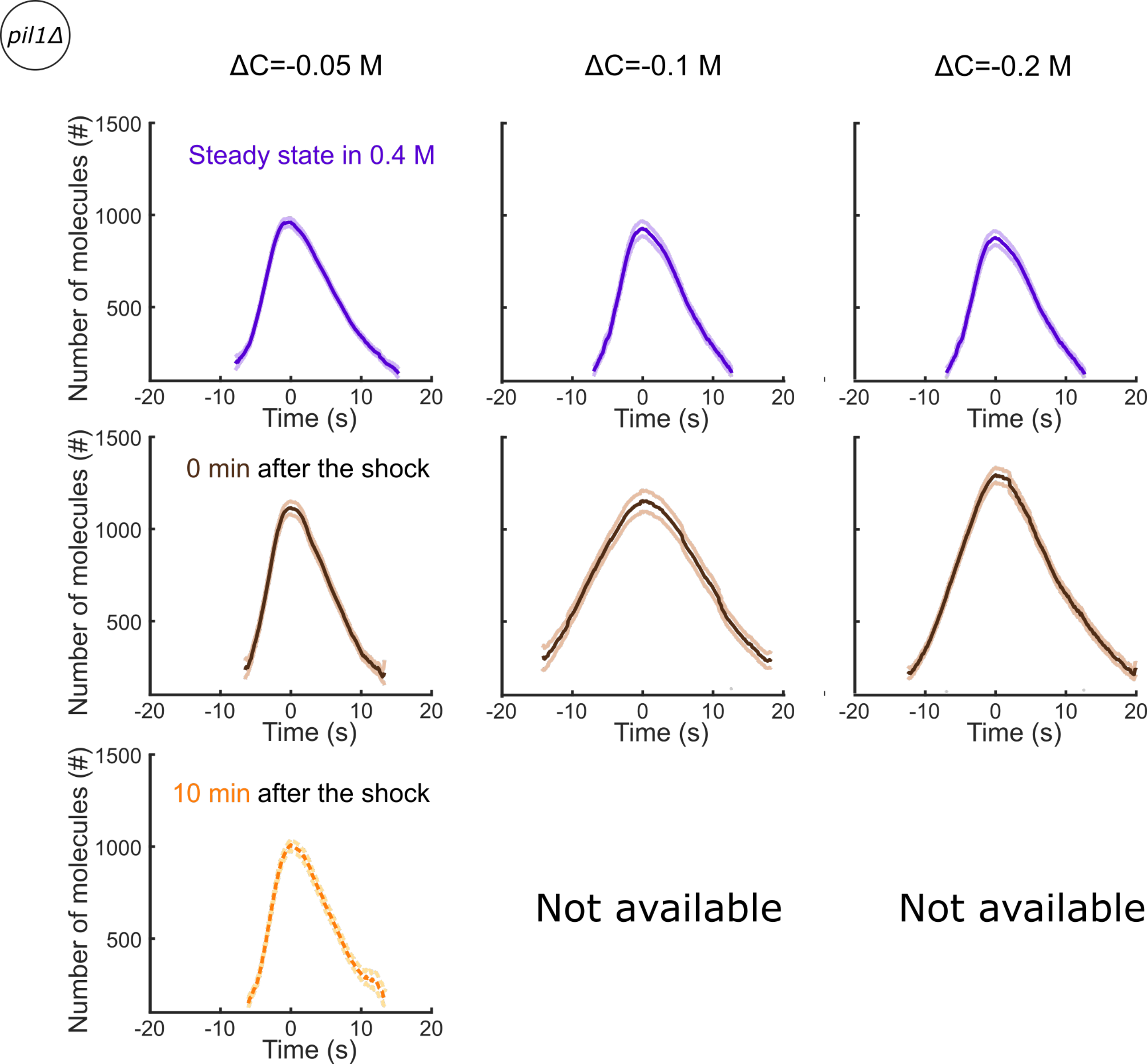

pil1Δ
ΔC=-0.05 M
ΔC=-0.1 M
ΔC=-0.2 M
Steady state in 0.4 M
0 min after the shock
10 min after the shock
Number of molecules (#)
1500
1000
500
-20
-10
0
10
20
Time (s)
Not available
Not available

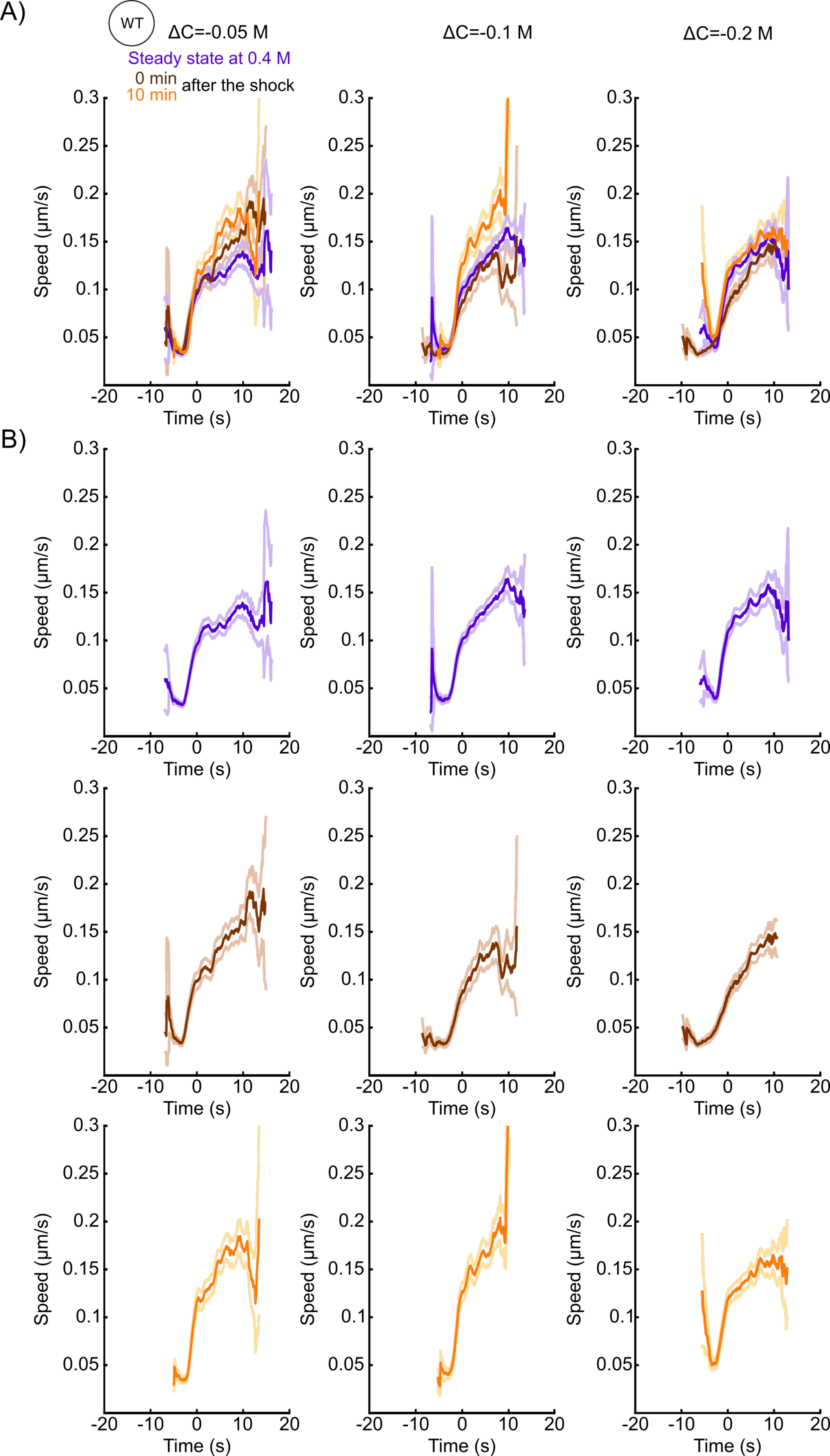
A)
WT
ΔC=-0.05 M
ΔC=-0.1 M
ΔC=-0.2 M
Steady state at 0.4 M
0 min
10 min
after the shock
Speed (μm/s)
Time (s)
B)

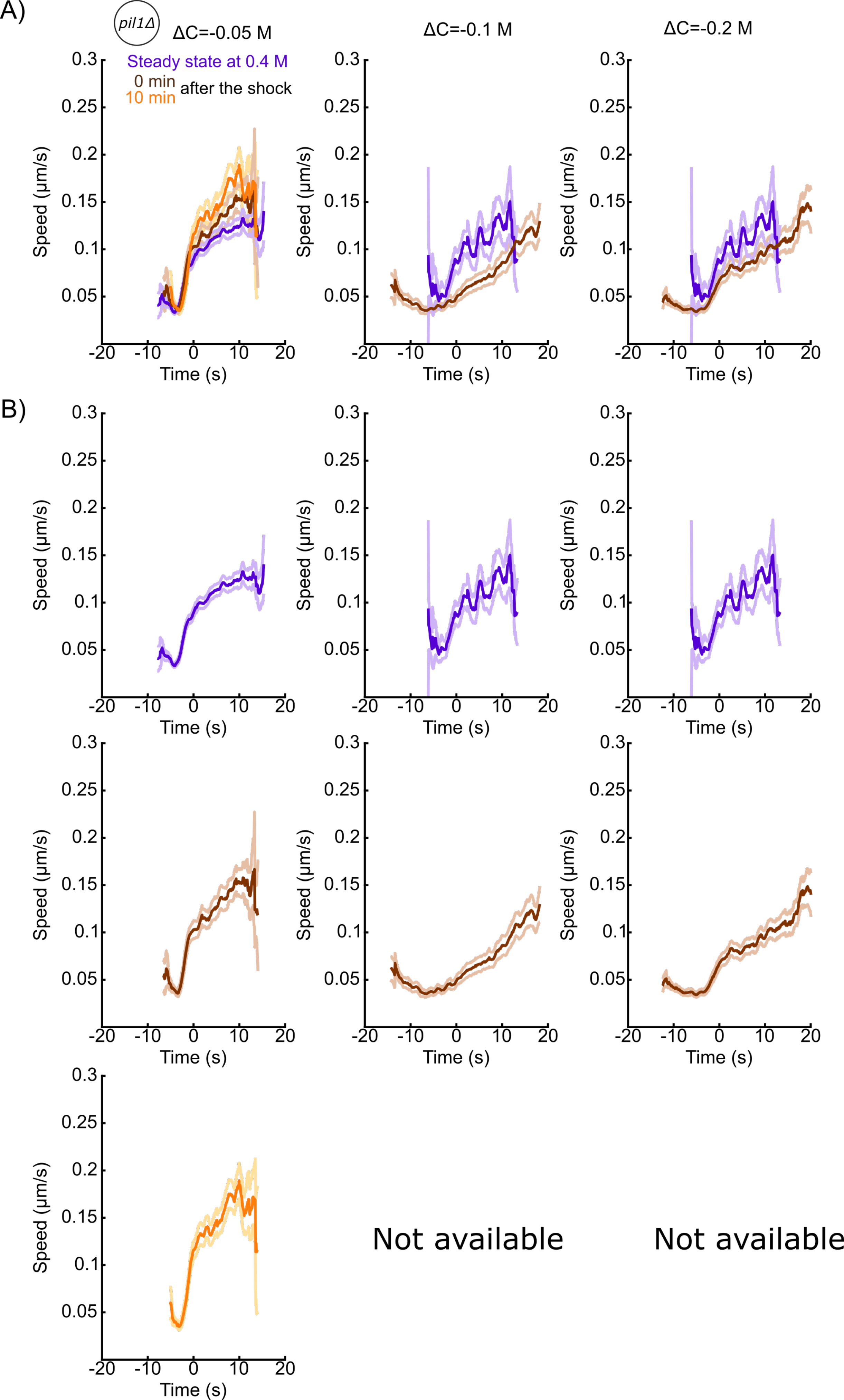
A)
pil1Δ
ΔC=-0.05 M
ΔC=-0.1 M
ΔC=-0.2 M
Steady state at 0.4 M
0 min
10 min
after the shock
Speed (μm/s)
Time (s)
B)
Not available
Not available

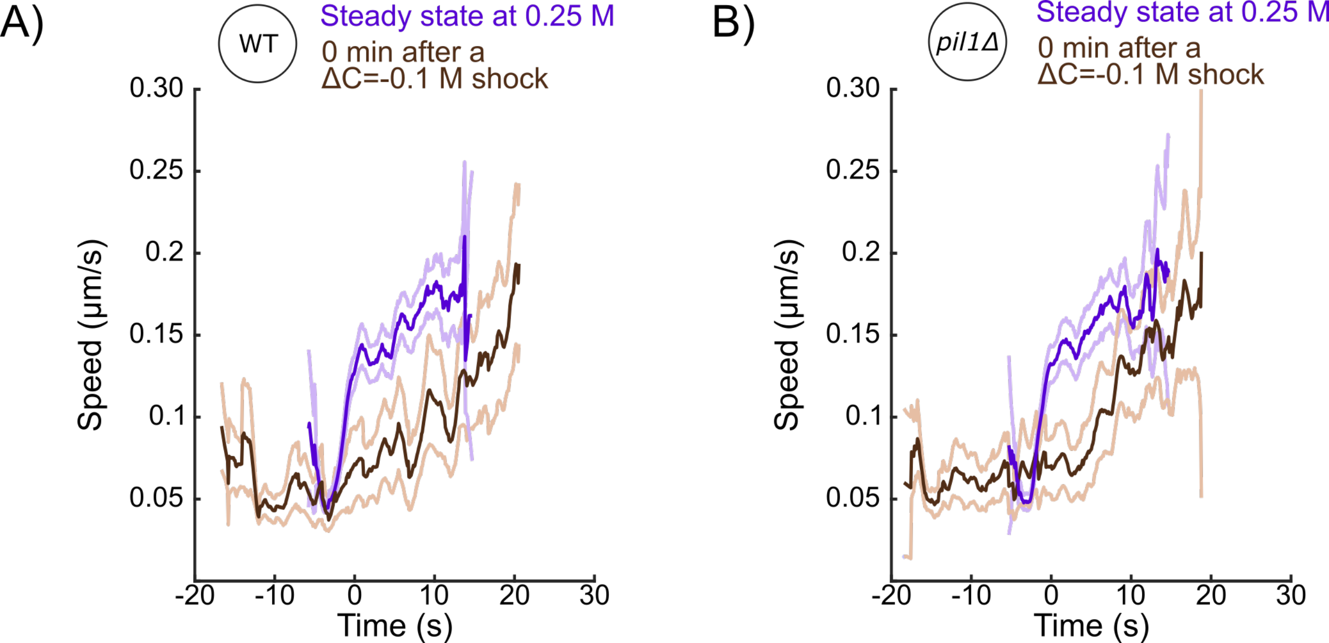

A)
WT
Steady state at 0.25 M
0 min after a
ΔC=-0.1 M shock
Speed (μm/s)
0.30
0.25
0.2
0.15
0.1
0.05
-20
-10
0
10
20
30
Time (s)
B)
pil1Δ
Steady state at 0.25 M
0 min after a
ΔC=-0.1 M shock
Speed (μm/s)
0.30
0.25
0.2
0.15
0.1
0.05
-20
-10
0
10
20
30
Time (s)